IMPACT OF CAPILLARY PRESSURE AND CRITICAL PROPERTIES SHIFT DUE TO CONFINEMENT ON HYDROCARBON PRODUCTION FROM SHALE RESERVOIRS

A THESIS SUBMITTED TO THE DEPARTMENT OF ENERGY RESOURCES ENGINEERING

OF STANFORD UNIVERSITY

IN PARTIAL FULFILLMENT OF THE REQUIREMENTS FOR THE DEGREE OF MASTER OF SCIENCE

By

Batool Arhamna Haider

August 2015

I certify that I have read this report and that in my opinion it is fully adequate, in scope and in quality, as partial fulfillment of the degree of Master of Science in Petroleum Engineering.

_____

Prof. Khalid Aziz (Principal Advisor)

Abstract

Interest in understanding the underlying physical mysteries that result in production through liquid rich shale reservoirs, is growing globally. A swiftly expanding branch of science termed as 'nano-fluidics' deals with studying fluid flow in nano-spaces and often accompanies computationally expensive molecular simulations. Compositional modeling of hydraulically stimulated naturally fractured liquid-rich shale (LRS) reservoirs is a complex process that is yet to be fully understood. This work aims to explore and integrate some of the key fundamentals of confined fluid flow in nano-pores with a fully compositional reservoir simulator.

Two phenomena, capillary pressure and critical property shifts, that become significant due to multiphase flow in nano-pores have been singled-out from various potential forces that arise at such small scales. LRS modelling capability of Automated Differentiation based General Purpose Research Simulator (AD-GPRS) was extended by making capillary pressure a function of pore radius. This was done by modifying vapor liquid equilibrium calculations to incorporate phase pressure differences that arise in tight pores. Using this formulation, fluid phase behavior properties were studied first using simple binary mixtures and later extended to a Bakken fluid sample. Our findings indicated that capillarity is a function of several phenomena which include pore size, fluid composition and reservoir pressure. Additionally capillary pressure was found to lead to bubble point suppression, reduction in oil density and viscosity, and increase in gas density and viscosity. Bakken fluid phase properties were found to deviate from bulk behavior up till pore radii of approximately 100 nm.

The study was then extended to a realistic hydraulically fractured shale reservoir model with a horizontal producer, and cases were run using Bakken fluid model. Reinforcing the findings of fluid phase behavior observed for simpler systems, oil production showed an increase, while gas production decreased as the pores got tighter. As expected, this change in production was found to be zero when the reservoir pressure is above the fluid bubble point pressure. However, a significant difference in hydrocarbon production and recovery due to capillarity was seen when the reservoir pressure fell below the bubble point pressure. Additionally, the importance of properly characterizing fractures was found to be important as their presence reduces the influence of capillarity. Further on, since shale reservoirs can contain pores of sizes ranging from <50 nm (nano and meso-pores) to >100 nm (micro-pores), two realistic pore size distributions (PSD) that are typically found in shale reservoirs were explored. The differences in production showed that capillary pressure is uniquely tied to the specific PSD of the reservoir. Moving further from the impact of pore size, the impact of varying fluid composition on the impact of capillary pressure was tested next. Since, many shale reservoirs such as Eagle Ford, contain a wide spectrum of hydrocarbon fluids ranging from low GOR black oil to volatile, rich and lean gas condensates, wet gas and even dry gas, and since these fluid compositions have been shown

to vary spatially within the play, the findings of this work are important. Bakken fluid composition was varied by increasing the compositions of light, mid-heavy and heavy components turn by turn. It was found that the impact of capillarity varies with the initial shape of the fluid mixture phase envelope. The lower the initial critical pressure, the greater will be the impact of capillarity. In Bakken's case, the magnitude of capillarity increased from relatively lighter compositions to mid-heavy compositions and then decreased again as the amount of heavier components was increased.

Finally, the impact of confinement on critical properties was studied. Using the correlations developed using molecular simulations that have been published previously, shift in critical properties of Bakken fluid sample were computed. Both critical temperature and pressure reduced as the pore size was decreased. It was shown that this reduction is greater for heavier components. We next ran simulations using the shifted critical properties. Both oil and gas production showed an increase.

Acknowledgments

This thesis marks the end of a great chapter of my life and the beginning of several stellar possibilities. My two years at Stanford have changed my life and the knowledge I have gained will certainly brighten my future paths like never before. My thanks to Energy Resources Engineering, Reservoir Simulation Industrial Affiliates (SUPRI-B) program and ENI for funding my MS and Stanford Summer Tutorial program which gave me one of the best experiences of lecturing Stanford students in my final quarter of MS.

I would like to thank Dr. Khalid Aziz who accepted me as his student and guided me throughout this research. To have worked with him was such a great privilege. When I had come to Stanford, I may not have been the best student in our batch, but towards the beginning of my second year, I was well determined to produce one of the best MS theses submitted in our year. I would like to thank Denis Voskov, who is extremely knowledgeable and his suggested directions were very important to my research. My heartfelt thanks to Dr. Huanquan for his great tips and advices, which made me re-do my results over and over again. I am very grateful to Sergey Klevtsov, who was the one you actually got be started with AD-GPRS. My initial progress with AD-GPRS would not have been so rapid had it not been for him. Finally I would like to thank Sergey Chaynikov for the many hours he spent listening to my issues and advising me about the possible strategies to ponder over. He has always been available on just an email of mine. I would also love to mention some of the awesome people I met at Stanford- my office mates and other friends which include Fatemeh Rassouli, Karina Lenevo, Mehrdad Shirangi, Sumeet Trehan, Humberto Samuel, Shaghan Kaur, Priyanka Dutta, Praveen Bains, Ghena Alhanie and Parwana Fayyaz. And finally, lots of thanks to our administrative staff Joanna Sun, Rachael Madison, Kay Wanglin and Eiko Rutherford!

My immense gratitude goes to my very beloved husband, Dr. Zeeshan Syedain, who is a great inspiration and a beautiful gift of God to me, for running back and forth from Minnesota to California so as to make sure my studies/career were going well. I would love to mention my two beautiful siblings, Ali and Kanza, who are the two joys of my life. My thanks to my in-laws who have been my home away from home and to my beloved grandmother, uncle and cousins in the US.

Most importantly, I would like to express my immense love and thank my very beloved Ammi (mom) and Abbu (dad), who are my two guardian angles. Nothing was possible without them, including my very existence.

Above and beyond all, I would want to thank my dear God who made my dreams come true in the most unexpected ways. I pray to Him that my dreams only grow bigger and that I become better to accomplish them all.

Contents

List of Tables

List of Tables

List of Figures

Chapter 1

1.Introduction

1.1. Introduction to this Thesis

Even though there is an abundance of shale resource globally, the underlying physics behind multiphase fluid flow in tight pore reservoirs has yet to be fully understood. This thesis aims to explore some of the key forces that become important at nano-scale of shale pores and the impact they have on hydrocarbon production in liquid rich shale reservoirs.

Following introduction to this thesis, Chapter 1 gives an account on the distribution of shale resources globally. It highlights the top shale oil and gas producers, the momentum of shale exploration world-wide and the speculated contribution of tight oil in the future energy scenario. This is followed by description on the types of fluids in shale reservoirs and genesis of liquid in shale pores. Finally, the chapter ends with a brief discussion on the variety of pore structures typically found in shale reservoirs and highlights the importance of pore size distribution towards characterizing fluid flow in shale reservoirs.

Chapter 2 offers literature review on the past work that has been done to investigate the impact of confinement on fluid flow. This chapter begins by offering details on the basic science of confinement and discusses three potential phenomenon that become significant due to confinement in liquid rich tight pore reservoirs, namely, capillary pressure, diffusion and shift in critical properties. An account has been presented on the Equation of State (EOS) method which can be modified to capture the impact of confinement, when modelling large scale reservoirs. The chapter ends with discussion on the importance of modelling desorption phenomenon in liquid rich shale (LRS) reservoirs.

Chapter 3 offers a detailed description of pertinent concepts of thermodynamics and how some of these principles can be modified to incorporate capillary pressure in current simulators, so as to extend their capabilities towards modeling LRS reservoirs better. Chapter 4 presents the results related to fluid phase behavior that have been obtained after incorporating capillary pressure in vapor-liquid equilibrium computations, as described in Chapter 3. Chapter 5 illustrates the tests done on the implemented capillary pressure formulation, so as to extend this implementation to realistic reservoir scenarios.

After successful trials in Chapter 5, Chapter 6 extends this formulation to a multi-staged hydraulically fractured reservoir scenario with a producing horizontal well. Several scenarios were set up to test the impact of capillary pressure on hydrocarbon production. These include cases with varying pore radii, reservoir pressure, and fluid compositions and pore size distribution. Finally, results related to the impact of critical property shifts due to confinement on hydrocarbon recovery have been presented.

Chapter 7 discusses some of the areas that need more investigation to further improve the modelling of capillary pressure in tight pore reservoirs. These include proper characterization of fractures and development of a reasonable porosity, permeability and pore size correlation.

Chapter 8 finishes this thesis by presenting the gist of this research work and offering directions to future researches on this subject matter.

1.2. Shale Oil and Gas 'Demographics'

Shale resources have been changing the world's energy equation. According to Energy Information Administration (EIA, 2013), estimated shale oil and shale gas resources in the United States and in 137 shale formations in 41 other countries represent 10% of the world's crude oil and 32% of the world's natural gas which is technically recoverable. This accounts for 345 billion barrels of technically recoverable shale oil and 7299 trillion cubic feet of recoverable shale gas in the world (EIA, 2013). Figure 1-1 shows the unconventional oil deposits world-wide, which include oil shale, extra-heavy oil & bitumen and tight oil & gas.

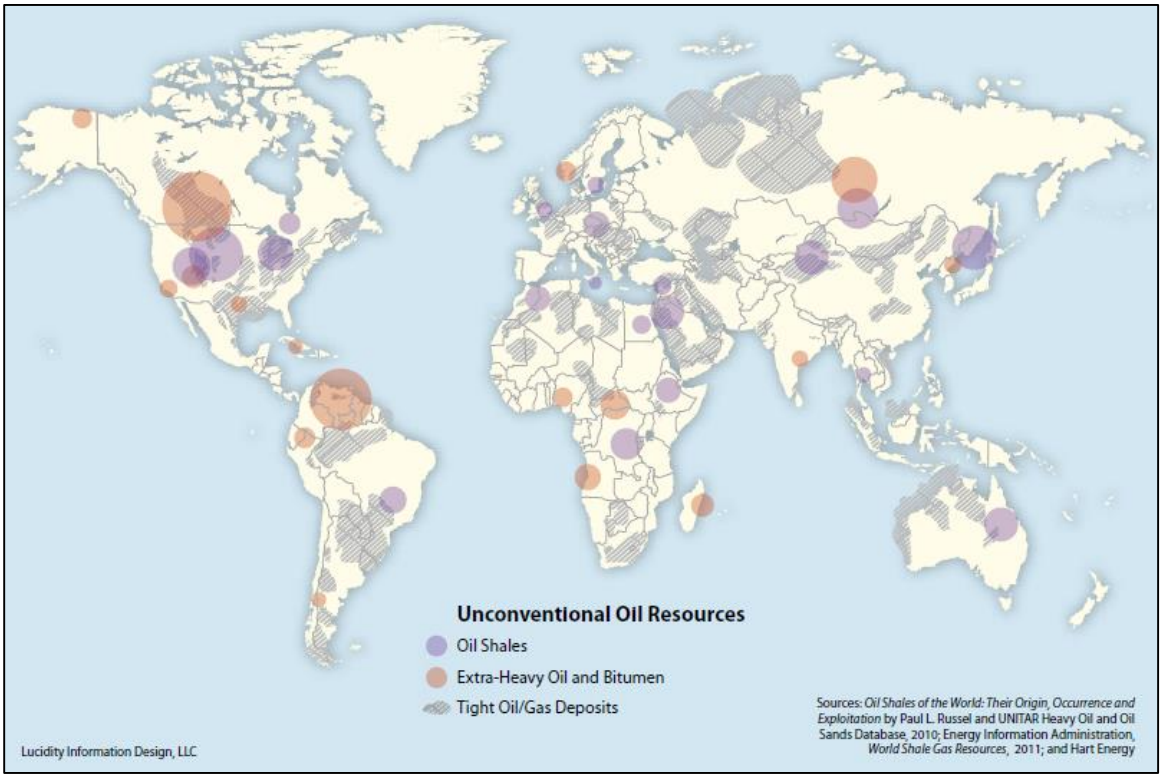

Figure 1- 1 Unconventional Oil Resources across the globe (Gordon, 2012)

Each of the fossil fuel energy resources comes with its own value. Figure 1-2 shows the API and value in BTU of different oil and gas types. Figure 1-3 on the other hand, illustrates the projected contribution of various hydrocarbon types. Unconventional oil includes heavy and extra heavy oil, while conventional and tight oil have been lumped into "Conventional and Transitional Oil.

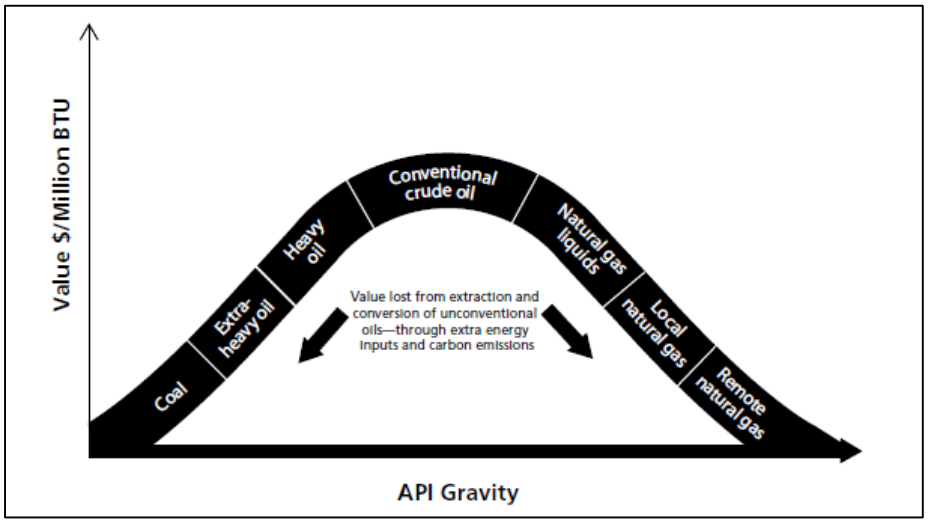

Figure 1- 2 Hydrocarbon Value Hierarchy (Gordon, 2012)

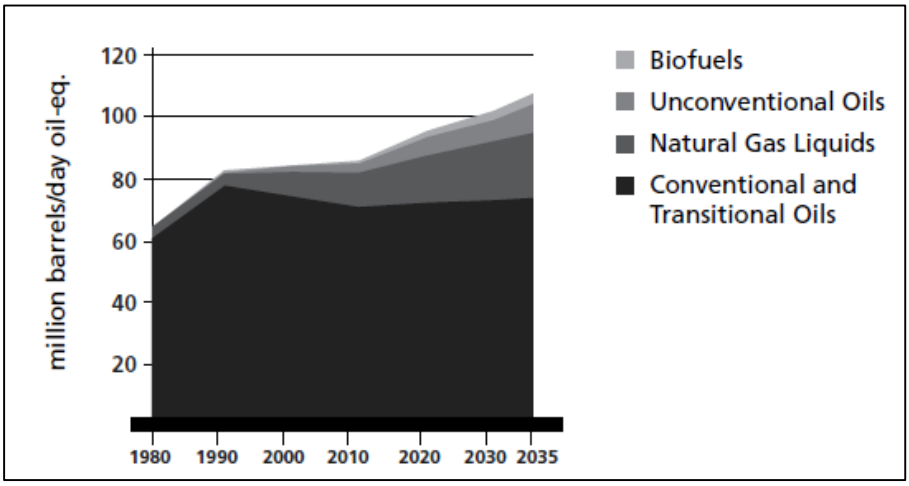

Figure 1- 3 Projected new oil scenario (Gordon, 2012)

Figure 1-4 shows some of the important light tight oil basins across the world and Figure 1-5 describes global shale resource exploration and extraction momentum in selected countries. While shale resources exploration has been banned by many countries in Europe, North America has progressed a lot in this direction. On the other hand Russia, China and Australia have begun exploration of their shale resources.

Figure 1- 4 Selected light tight oil plays world-wide (Schlumberger (2015)

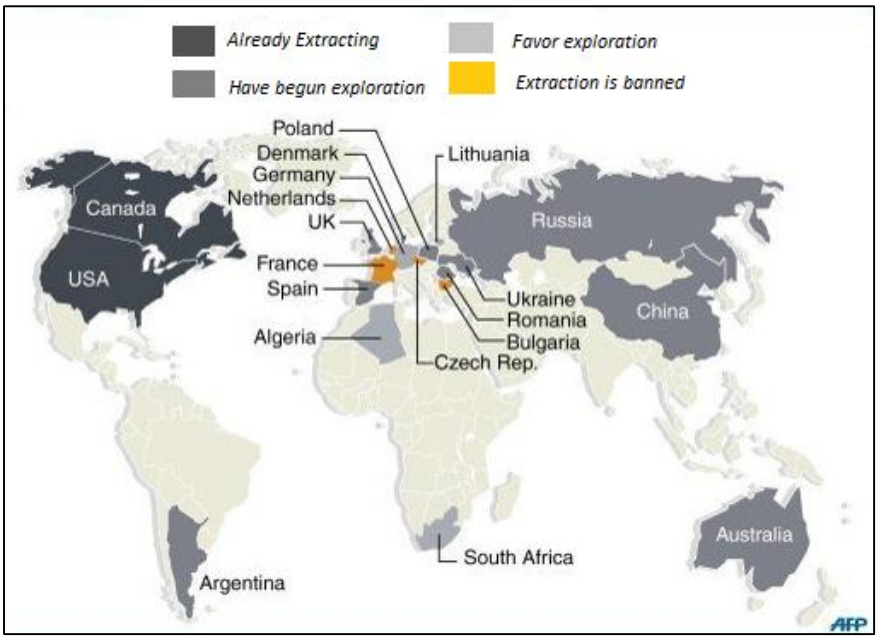

Figure 1-5 Approach of selected countries towards shale resource exploitation (Pouchot, 2013)

Table 1-1 ranks countries by the amount of technically recoverable shale oil and gas they bear. With 75 Billion Barrels of shale oil, Russian tops the list of Shale oil reserves while China tops the list of shale gas reserves. It is interesting to see how small countries like Pakistan too have emerged as lands rich in shale oil reserves.

Table 1-1 Top 10 countries with technically recoverable shale gas and oil reserves (adopted from EIA (2013))

Rank	Country	Shale Oil (Billion Barrels)	Country	Shale Gas (Trillion Cubic Feet)
1	Russia	75	China	1115
2	United States	58	Argentina	802
3	China	32	Algeria	707
4	Argentina	27	U.S.	665
5	Libya	26	Canada	573
6	Australia	18	Mexico	545
7	Venezuela	13	Australia	437
8	Mexico	13	South Africa	390
9	Pakistan	9	Russia	285
10	Canada	9	Brazil	245

Figures 1-6 and 1-7 show the ranking of continents in terms of shale oil and gas reserves and in place resources, respectively. The charts have been constructed using information extracted from EIA (2013). Europe tops the list of shale oil reserves and resource in-place, followed by Asia and South-America. On the other hand, Africa and South America, top the list of shale gas in-place and technically recoverable shale reserves, respectively.

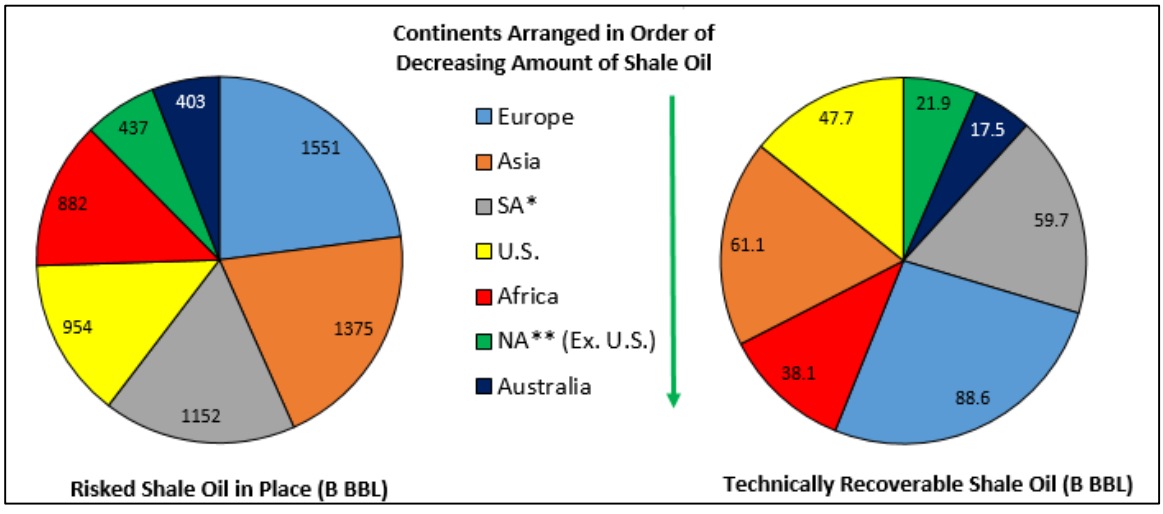

Figure 1-6 Continent-wise breakdown of risked in-place and technically recoverable shale oil (information source (EIA, 2013))

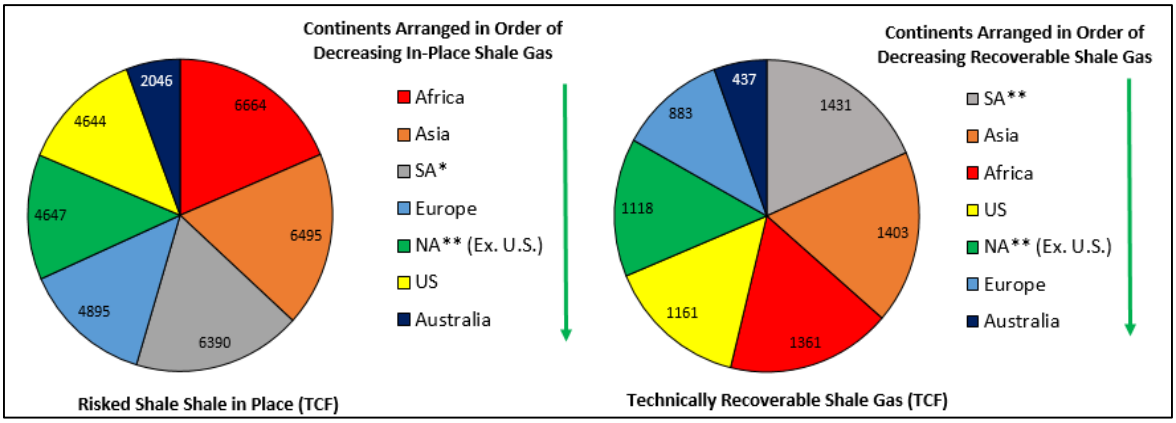

Figure 1-7 Continent-wise breakdown of risked in-place and technically recoverable shale gas (information source (EIA, 2013))

* SA is South America
** NA is North America (here excludes USA)

1.3. Types of fluids in Shale Reservoirs and Genesis of Liquid in Shale Pores

Shale resources can be broadly classified into 3 categories- Oil Shale, Shale Oil and Gas Condensate (often termed as Liquid Rich Shale (LRS) fluids) and Shale Gas. Each of these differ greatly in flow characteristics. According to Colorado Oil and Gas Association (COGA, 2013), oil shale contains remains of "algae and plankton deposited millions of years ago that have not been buried deep enough to become sufficiently hot in order to break down into the hydrocarbons targeted in conventional oil projects". Shale oil and gas on the other hand, are formed when the rock is buried deep enough to convert part of its kerogen into oil and gas. Horizontal drilling and fracturing is often required to produce them commercially, because these hydrocarbons are locked in place very tightly (COGA, 2013). We shall concentrate on this second class of shale resource, that is, on Liquid Rich Shale (LRS) reservoirs.

Several aspects determine whether Shales are capable of generating hydrocarbons and whether they will generate oil or gas. During the process of hydrocarbon formulation, first oxygen evolves as kerogen gives off CO_2 and H_2O, and later hydrogen evolves as hydrocarbons are formed (McCarthy, 2011). The general trend in the thermal transformation of kerogen to hydrocarbon starts with the generation of non-hydrocarbon gases and then progresses to oil, wet gas and dry gas (McCarthy, 2011). Figure 1-8 illustrates this progression for different types of kerogen. During thermal maturity of type I kerogen, liquid hydrocarbons tend to be generated. Type II on the other hand, generates gas and oil, while type III generates gas, coal (often coal bed methane) and oil in extreme

conditions. It is generally considered that type IV kerogen is not capable of generating hydrocarbons (Rotelli, 2012). Figure 1-9 highlights the conditions required to generate liquid hydrocarbons. Physical and chemical alteration of sediments and pore fluids take place at temperatures of 50 C – 150 C (Pederson, 2010). This process is called "catagenesis". At these temperatures, chemical bonds break down in kerogen and clays within shale, generating liquid hydrocarbons (Pederson, 2010).

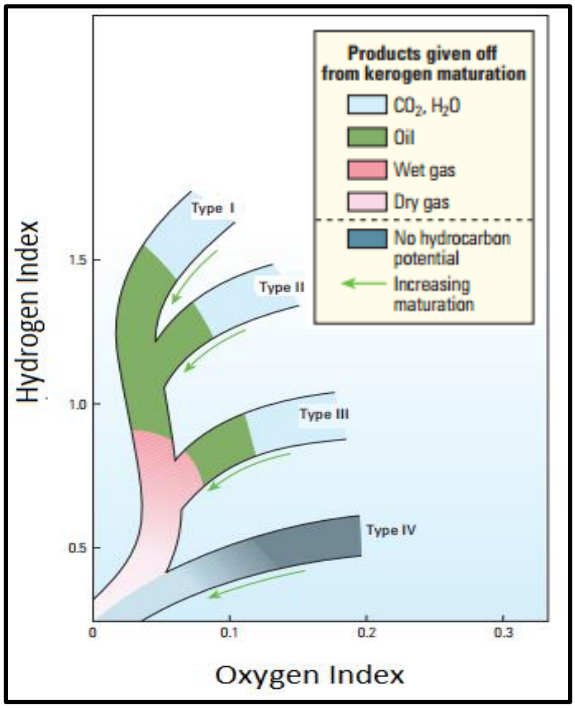

Figure 1-8 Kerogen type and Oil & Gas formulation (McCarthy, 2011)

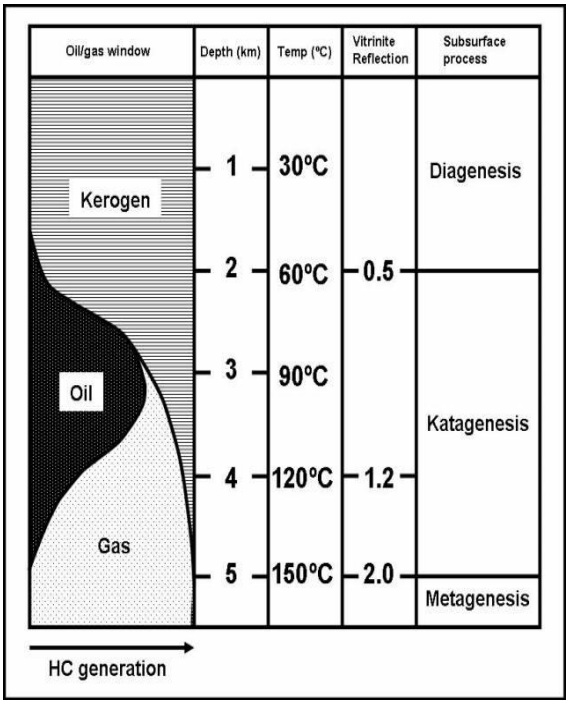

Figure 1-9 Depth & Temperature condition for Oil and Gas Formulation (Pederson, 2010)

Liquid Rich Shale (LRS) fluids can be divided into two categories- Shale Oil and Shale Gas Condensate. At the original reservoir conditions, a gas-condensate is a single-phase fluid (Fan, 2005). According to the work of Ismail (2010)**,** shale condensate systems consist predominantly of "methane (C1) and other short-chain hydrocarbons. The fluid also contains small amounts of long-chain hydrocarbons (heavy ends). The methane content in gas-condensate systems ranges from 65 to 90 mol%, whereas in crude oil systems, methane content ranges from 40 to 55 mol%". Figure 1-10 shows a ternary diagram of these classifications.

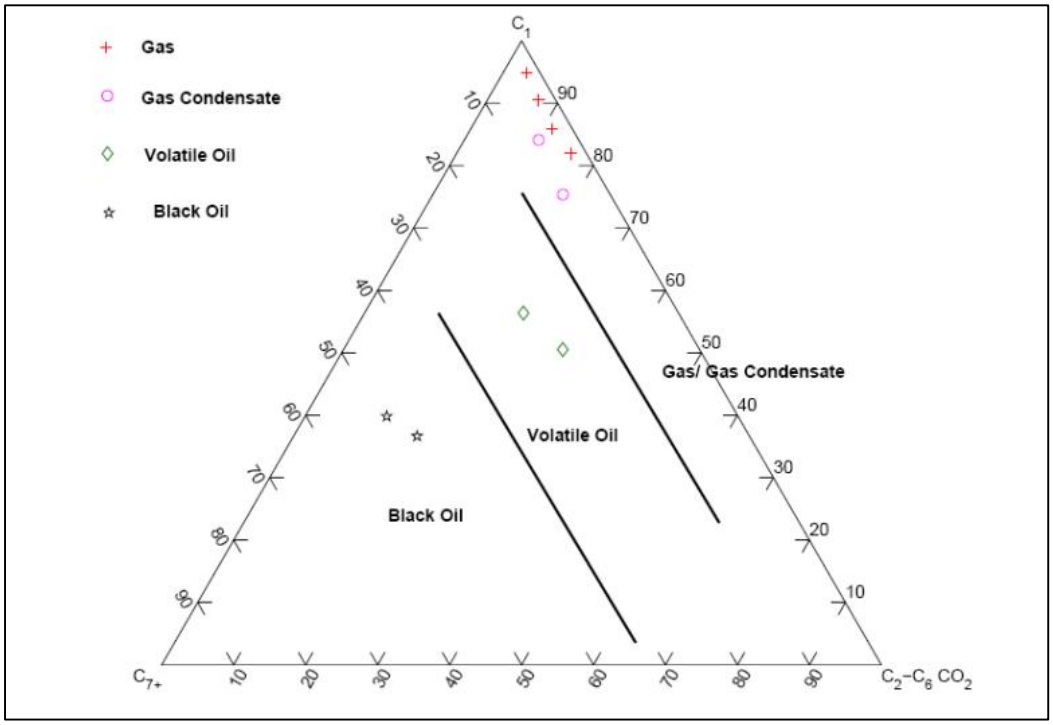

Figure 1-10 Ternary visualization of hydrocarbon classification (taken from Ismail (2010). Original source is Whitson (2000).

1.4. Shale Pore Structure and Heterogenity

The average size in currently producing liquid rich reservoirs is estimated to be less than 100 nm (Firincioglu, 2014). According to Rotelli (2012), in-order to properly characterize shale, it is important to understand the following:

- Volume of pore network
- Characteristic dimension of pore network
- Pore type predominantly present
- Complexity of pore network

Based on the work of Kuila (2013), small pores in a shale matrix are associated with clay and kerogen. Bustin (2008) reported a bi-modal pore size distribution with modes around 10 nm and 10,000 nm for Barnett and Antrim formations. Loucks (2012) showed that scanning electron microscope (SEM) images of nanometer scale pores associated with clays and kerogen in Barnett shale, revealed pores as small as 4nm. Sondergeld (2013) stated that shale reservoirs exhibit hydrocarbon storage and flow characteristics that are "uniquely tied to nano-scale pore throat and pore size distribution". Figure 1-11 shows the

different types of pores present in shale reservoirs. Each of them may alter fluid flow in a different manner.

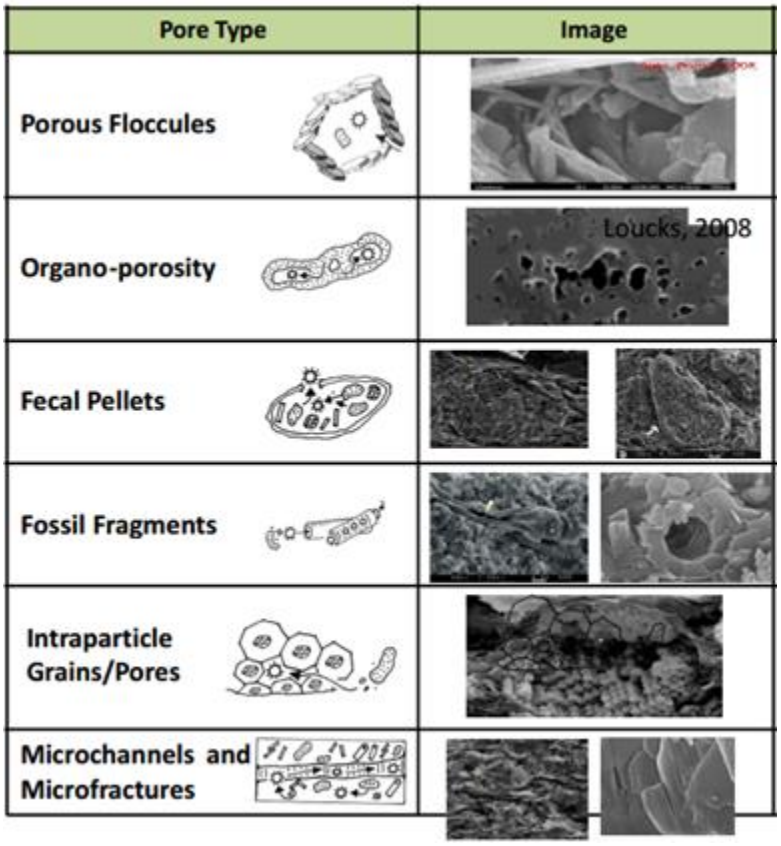

Figure 1-11 Pore types in the Barnett and Woodford gas shales (Slatt, 2011)

1.5. Summary

This chapter presented a high level overview of shale resources globally, the conditions that are required to turn kerogen into liquid hydrocarbons, and types of fluids and pore structures that can be found in shale rocks. In the next chapter, we shall delve deeper into some of the intricacies affiliated with multiphase fluid flow in nano-pores of shale reservoirs.

Chapter 2

2. Potential Forces influencing Storage and Flow of Fluid in Liquid Rich Shale Reservoirs

Various forces that are insignificant at bulk scale can be of considerable importance at nano-scale and so can no longer be ignored. This Chapter discusses the science of confinement and offers review on the work done by various authors to investigate the impact of confinement on fluid flow. Three of potential phenomena that become significant due to confinement in liquid rich tight pore reservoirs, have been focused on. These are capillary pressure, diffusion and shifts in critical properties, alongside liquid adsorption/desorption which can be an important storage mechanism in shale pores.

2.1 Confined fluid flow in Liquid Rich Shale Reservoirs

Fluid transportation and phase behavior under confinement exhibit significant deviations from their corresponding bulk behavior (Sanaei, 2014) (Travalloni, 2010) (Devegowda, 2012) (Kuz, 2002). Experiments conducted by (Ismail, 2014) at Stanford University on gas condensate systems showed that liquid rich shale gas composition varied along the direction of flow during depletion. The change in gas composition was concluded to be a result of condensate dropout and relative permeability effects. More importantly, the variation in gas composition in Marcellus shale core was less than that in the Berea sandstone core. This was an indication that the amount of condensate dropout varies between shale and sandstone for the same fluid system and at similar flowing conditions. Hence, the phase behavior is affected by the additional fluid-rock interaction expected for shale due to flow through nanometer sized pores (Ismail, 2014). Nojabaei (2012) showed that accounting for bubble point suppression due to confinement gave a better match between the gas production data and simulator predictions for a well in Bakken field. Sanaei (2014) studied an Eagle ford sample in condensate window and showed that reduction of the pore size down to the order of nano-scale led to the shrinkage of two-phase region, causing reduction in condensate drop-out and near wellbore permeability impairment. After 10 years of production, condensate saturation around Stimulated Reservoir Volume (SRV) was found to be 6-10% less under confinement effects.

Therefore it is important to understand the fundamentals of confined fluid flow in order to decipher the mechanisms via which multiphase fluid transport takes place in liquid rich shale reservoirs.

2.2 Basic Science behind Confinement

In a porous solid with interconnected pathways, a molecule may collide with another molecule or with the pore walls. When the pore size is relatively larger, the number of interactions the molecules have with the pore walls is negligible as compared to the number of interactions molecules have with one another. This however does not hold true as the pore size gets smaller (Chandra, 2014). In tight reservoirs, pore sizes become comparable to the size of the fluid molecules trying to flow through them (Nelson, 2009). Figure 2-1 illustrates this effect schematically. The red particles indicate the molecules that get to interact with the pore wall at a given time. Since a nano-pore can hold fewer molecules when compared to macro-pores, the interaction amongst molecules (van der Waals interactions) and between molecules and the pore wall increases. Fluid molecules in such a condition are termed to be 'confined' or under 'pore proximity' effect because the free path available to the molecules is restricted by the geometry of the void space of pore (Chandra, 2014). Roughly speaking, confinement effect is felt when the pore size to molecule size ratio is less than 20 (Devegowda, 2012). Pore throat diameter that is typical in shale gas formations have been shown to vary between 0.5 -100 nm (Ambrose, 2010), while the chain diameter of straight hydrocarbons is in the range of 0.4 - 0.6 nm (Mitariten, 2005).

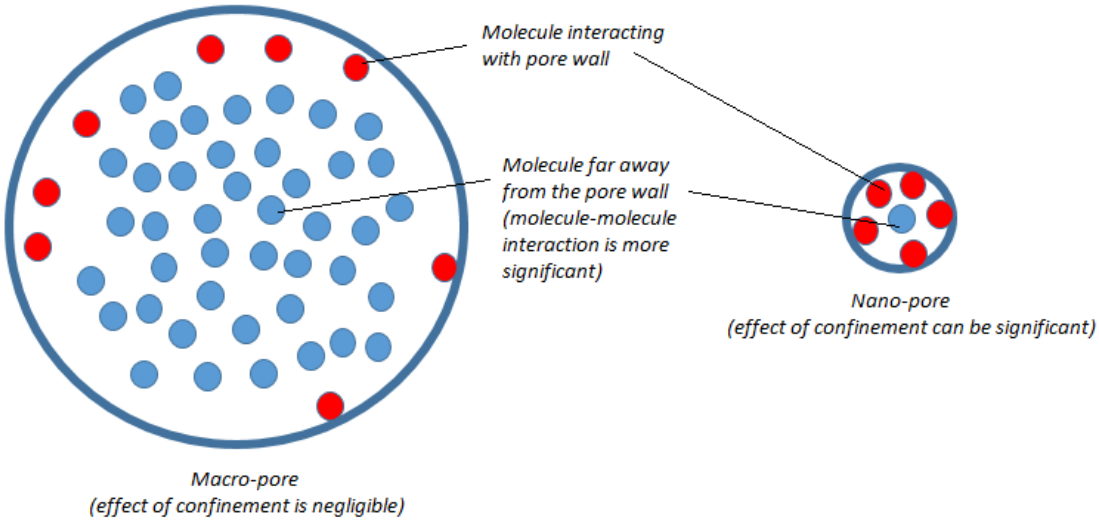

Figure 2- 1 Schematic representation of confinement effect

The properties of molecules in the surface layer (the ones close to the pore wall as indicated by molecules colored in red in Figure 2-1) would be affected by increased pore wall-fluid interactions, which leads to alteration in dynamics of molecules in the surface layer sticking to pore wall (Chandra, 2014). Overall, the situation of molecules in confined geometry is both theoretically and experimentally very complicated and not fully understood.

2.3 Impact of Confinement on Critical Properties

When phase envelope is crossed in gas condensate systems, there is a large gas oil volume split in the nano, meso and macro pores (Alharthy, 2013). This is presumed to be responsible for economical production of liquids in such systems. Simulations and experimental data reveal that critical properties of many compounds change as pore size decreases (Singh, 2009) (Devegowda, 2012). It was illustrated by Kuz (2002) that in order to properly account for the behavior in confined fluids, the critical properties of components should be altered as a function of the ratio of molecule to pore size. They developed a correlation for the deviation of critical temperature and pressure from van der Waals equation of state (EOS) by studying confined fluids in square cross section pores. Though they neglected the interaction between the fluid molecules and the wall, they did find good agreement between the predicted capillary condensation and critical temperature and experimental data.

Hamada (2007) used grand canonical Monte Carlo numerical simulations to study thermodynamic properties of confined Lennard-Jones (LJ) particles in slit and cylindrical pore systems and indicated changes in fluid phase behavior as a function of pore radius. Singh (2009) investigated the behavior of methane (C1), n-butane (C4) and n-octane (C8) inside nanoscale slits with widths between 0.8 to 5 nm using grand canonical Monte Carlo simulations and found out that while critical temperature decreased with reduction in pore radius, the critical pressures of n-butane and n-octane first increased and subsequently decreased. They also found that the critical property shift is dependent on pore surface types and hence differed for mica and graphite. This work is of importance as shale rocks are characterized by organic and inorganic pore systems, both of which vary in mineral composition and thus will cause different intensities of pore wall and molecules' interaction (Devegowda, 2012).

Teklu (2014) extended the work of Singh (2009) to Bakken fluid sample and founded that shifts in critical properties led to the suppression of Bakken fluid phase envelope. Alharthy (2013) also used the correlations developed by Singh (2009) to investigate the impact of confinement on various variations of Eagle ford composition. They found that shift in critical properties led to an increase in condensate production and this increase was a function of both pore size, as well as fluid composition.

2.4 Diffusion effect due to Confinement

Confinement may give rise to Knudson diffusion. As discussed previously, in a porous solid, a molecule may collide with another molecule or with the pore walls. At high pressure, molecule-molecule collisions are dominant. At low pressure, collisions are dominantly between molecules and the walls, and the free path is restricted by the geometry of the void spaces (Rotelli, 2012). This regime is termed as Knudson Diffusion. It combines both the geometry as well as the pressure information of the system. At low Knudson diffusion number the continuum flow regime is valid, but in the regime where Knudson is

approaching unity, possibly the continuum validity breaks down (Rotelli, 2012). The Knudson number is defined by:

$$K_n = \frac{\lambda}{L} \qquad \textbf{(2- 1)}$$

Here λ is the mean free path travelled by the fluid particle as shown in Figure 2-2, L is the pore diameter and K_n is Knudson number. The range of its values in different flow regimes is listed in Table 2-1.

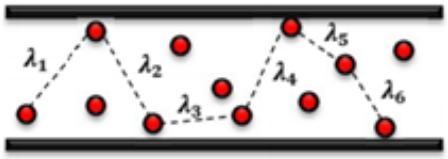

Figure 2- 2 Schematic illustration of the mean free path taken by molecules in confinement (Blasingame, 2013)

Table 2- 1 Flow regimes based on Knudson diffusion number (*info source* Kuila (2012))

Knudsen Number Range (K_n)	**Flow Regime**
$K_n \leq 0.001$	Viscous flow
$0.001 \prec K_n \prec 0.1$	Slip Flow
$0.1 \prec K_n \prec 10$	Transition flow
$K_n \geq 10$	Knudsen's (free molecular) flow

Rotelli (2012) showed that for gas condensates, diffusion can play an important role especially in small pore sizes and at lower pressures. In multiphase compositions, such as gas condensate reservoirs, the equilibrium gas composition at bubble point differs due to bubble point suppression. This will be discussed later in this thesis. Having differing gas compositions (at the bubble point) in different sized pores should impact the gas phase growth and may cause flow due to diffusion. Additionally, heterogeneity of the pore size distribution maybe one of the important reasons for concentration gradients causing diffusive flow in unconventional liquid rich reservoir (Firincioglu, 2014). Rotelli, (2012) showed that unlike gas condensates, oil is characterized by a more viscous flow, so it tends to move according to Darcy's equation. This is because in case of oil, molecules tend to interact with each other before they are able to reach the pore wall.

2.5 Capillary Pressure

Nano size pores can affect the phase behavior of in situ oil and gas owing to increased capillary pressure (Alharthy, 2013) (Nojabaei, 2014) (Wang, 2013). Not accounting for increased capillarity in small pores can lead to inaccurate estimates of ultimate recovery and saturation pressures. It has been argued that in the presence of capillary forces, the classical thermodynamic behavior is not sufficient to explain gas bubble formation in porous medium (Alharthy, 2013). When capillary forces are considered, the classical thermodynamics approach requires very high super saturation values that are typically not observed in conventional hydrocarbon reservoirs (Firincioglu, 2014).

In tight pore reservoirs, due to the fact that a relatively significant number of molecules get to interact with the pore walls, the pressure difference between the wetting phase (the phase that sticks to the pore walls) and the non-wetting phase can no longer be ignored. This gives rise to capillary pressure which is:

$$P_{cap} = P_{nw} - P_w$$

Here P_{cap} is the capillary pressure, P_w is the wetting phase pressure and P_{nw} is the non-wetting phase pressure.

Investigating the impact of capillary pressure is the prime focus of this work. Based on previously published literature, the presence of capillarity leads to a reduction in oil density and viscosity while an increase in gas density and viscosity (Nojabaei, 2012) (Firincioglu, 2014). Figure 2-3 shows the alteration of various fluid properties in the presence of capillary pressure. As shown, oil density reduces when capillary pressure becomes significant.

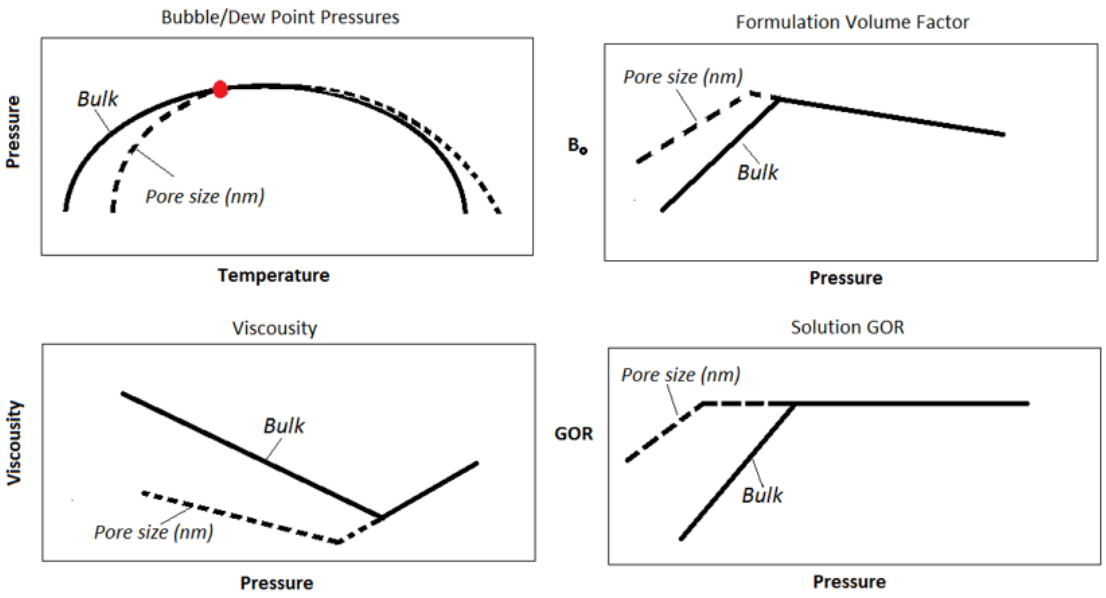

Figure 2-3 Alteration of fluid properties under the influence of capillarity (after Honarpour (2013))

Reduction in oil density and viscosity can be attributed to suppression of bubble point pressure, a phenomenon that arises under the influence of capillarity (Honarpour, 2013) (Nojabaei, 2012) (Alharthy, 2013) (Wang, 2013) (Teklu, 2014). Dew point on the other, appears at relatively higher reservoir pressures. The suppression of bubble point pressure causes gas to be in oil for a longer time as pressure is reduced. Figure 2-4a shows a schematic representation of the unconfined scenario when gas starts evolving as soon as the reservoir pressure drops below the fluid's bubble point pressure. Figure 2-4b on the other hand illustrates what happens when confinement makes capillary pressure significant, which in turn causes suppression of the bubble point. Compared to unconfined system, gas will stay dissolved in oil at lower pressures. This phenomenon is likely to cause an increase in oil production and recovery.

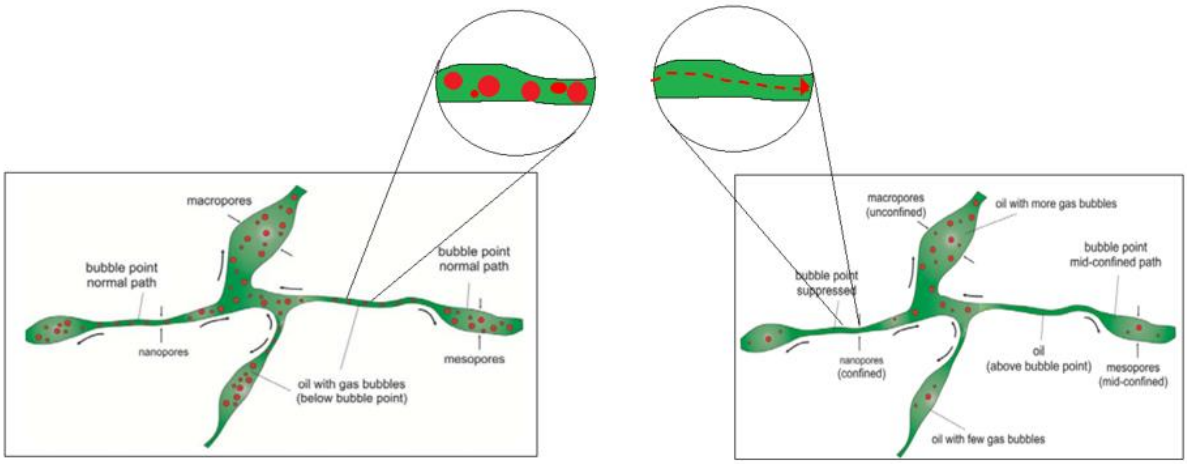

Figure 2- 4 Conceptual pore network model showing different phase behavior paths without and phase behavior shift (Alharthy, 2013), Left: 2-4 a, Right: 2-4 b

Nojabaei (2012) attempted to history match gas production data obtained from a well in the Bakken field using both suppressed bubble point and the original bubble point of the unconfined fluid. This is shown in Figure 2-5. It was observed that predictions matched the field data well with suppressed bubble point pressure by producing less gas compared to conventional unconfined systems. This indicates the strong need to further our understanding regarding the potential forces that alter the bubble point pressure in tight pores.

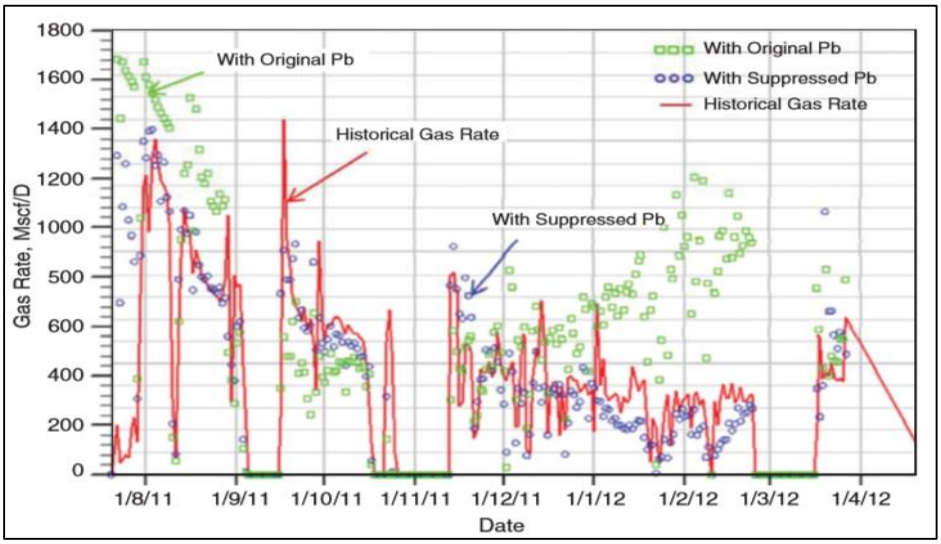

Figure 2- 5 History match of gas rate for scenarios with or without PVT adjustments (Nojabaei, 2012)

2.6 Equation of State for Fluids in Confinement

Since there are many uncertainties and challenges associated with laboratory based experimentation to determine the impact of confinement on phase behavior in nano-pores, attention has shifted to numerical studies (Ma, 2014). The popular numerical modeling approaches can be divided into three categories-

1. Equation of state
2. Molecular simulation
3. Density function theory

Usually, cubic equation of state (EOS) are used to calculate phase behavior of the hydrocarbon fluids. Such EOS include Peng-Robinson, Redlich-Kwong, Soave-Redlich-Kwong, and Zudkevitch-Joffe-Redlich-Kwong. The EOS parameters are generally determined by the calibration of the model to laboratory measurements, such as Constant Composition Expansion (CCE), Constant Volume Depletion (CVD), and Differential Liberation (DL), and separator tests (Firincioglu, 2014). These tests are performed in PVT cells without consideration of the porous media effects. Similarly, black-oil simulators use tabulated values of fluid properties that are measured under reservoir conditions in PVT cells (Firincioglu, 2014).

Several experiments using molecular simulation show alteration of fluid properties in confinement, that are critical to phase behavior (Singh, 2009) (Jiang, 2006). Although these methods improved our understanding of phase behavior of confined fluids, the computational demands of these approaches make them impractical for practical use. Other

proposed methods include the use of new or modified versions of existing equations of state in order to accurately model experiments. The EOS method in general tends to require less computational effort and consequently is more amenable for operational simulation problems (Ma, 2013).

The ideal gas law is the most simplistic relation between pressure, temperature, volume and amount of an ideal gas. Van der Waals equation may be considered as the ideal gas law "improved" due to two independent reasons - molecules are thought as particles with volume, not material points and while ideal gas molecules do not interact, van der waals consider molecules attracting others within a distance of several molecules' radii. Thus an extra term was added in the original ideal gas equation to account for the interaction between molecules (van der Waals, 1873). Peng Robinson and Soave Redlich Kwong equations were derived from Vander Waals (VDW) equation so as to account for fluid molecule-molecule attraction by modifying the attractive pressure term in VDW EOS (Vidal, 1997). When dealing with confinement, the interactions between the pore walls and molecules too become significant (Zhang, 2013). Many authors have focused on this fact to modify bulk EOS so as to make it more applicable to confinement conditions.

Zhu (1999) used the theory of thermodynamical interfaces to describe N2 adsorption in different sizes of cylindrical mesopores and developed an EOS that describes important features of adsorption process in meso-pores by accounting for attractive interactions between the adsorbed molecules and adsorbent, the curvature of adsorbed phase interface, and surface tension. They concluded that the smaller the pore radius is, the thicker the adsorbed film will be. This generally leads to capillary condensation. Schoen (1998) modified the VDW EOS by applying perturbation theory to confined fluid in slit-pores. Their EOS could predict capillary condensation and depression of critical temperature qualitatively. The predictions of the EOS were however found to be unsatisfactory in the vicinity of critical region (Ma, 2013). Zarragoicoechea (2002; 2004) extended VDW EOS to study confined fluids in square cross section pores. They assumed a tensorial character for the pressure of confined fluid and neglected the interaction between the fluid molecules and the wall. However, they did find good agreement between the predicted capillary condensation and critical temperature and experimental data. Derouane (2007) modified VDW EOS by introducing a new term that takes into account the attractions between the fluid molecules and the pore wall, and it based on pore size. Ma (2013) modified VDW EOS, by including the fluid molecule- pore wall interactions, besides the existing fluid molecule-molecule interactions. Their EOS can describe fluids phase behavior under confinement of any pore size- that is from bulk state (very large pores) to nanopores which result in confined state.

Travalloni (2010) presented an analytical equation of state that takes the effect of pore size and the interaction between the fluid molecules and the pore wall into account. They derived a generalized form of EOS for confined fluids by demarcating the confined pores into three different regions where predominant forces are likely to be different. In Region I, the fluid molecules are sufficiently far from the pore walls and consequently fluid behavior depends solely on inter molecular forces, while in Region 3, fluid molecules are influenced strongly by the pore walls. Figure 2-6 illustrates this demarcation.

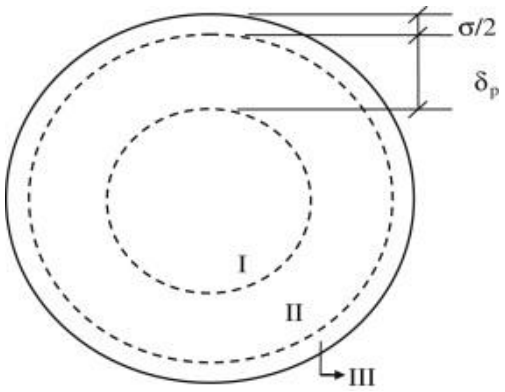

Figure 2-6 Regions inside a pore defined by molecule-wall interaction potential (Travalloni, 2010)

2.7 Adsorption Phenomenon in Liquid Rich Shale Reservoirs

In dry gas shale reservoirs, it is widely acknowledged that gas adsorption is one of the most important storage mechanisms, and that it accounts for close to 45% of initial gas storage (Rajput, 2014). In case of liquid rich shales however, typically adsorption is not considered. Using adsorption modelling formalism based on thermodynamically Ideal Adsorbed Solution (IAS) theory, Rajput (2014) showed that 5-13% of the liquid fluid present in shale can be adsorbed onto shale and negligence of this additional storage mechanism can lead to considerable error in reserve estimation. The error values depend on the amount and adsorption parameters of adsorbent present, as well as the composition of liquid rich shale. Figure 2-7 shows the differences in critical and dew point line of the phase envelopes of fluid mixtures, with and without consideration of liquid phase adsorption. There is however insignificant change in bubble point line location which could be attributed to the fact that heavier components are preferentially adsorbed.

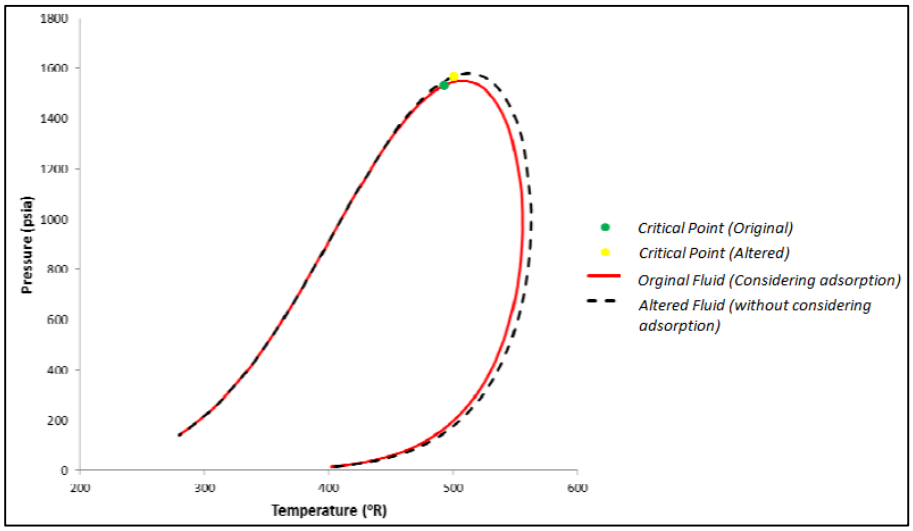

Figure 2- 7 Comparison of phase envelopes of original and adsorption altered reservoir fluid (Rajput, 2014)

Haghshenas (2014) modelled heavy hydrocarbon component adsorption using Langmiur isotherms. Figure 2-8 shows that for hydrocarbon components, adsorption increases strongly with the molecular weight. This observation shows that in liquid rich shales, adsorption on organic matter may be an important storage mechanism for the heavier fractions. Haghshenas (2014) also showed that the contribution of liquid desorption to the overall hydrocarbon recovery was dependent on fluid composition and pore connectivity/configuration.

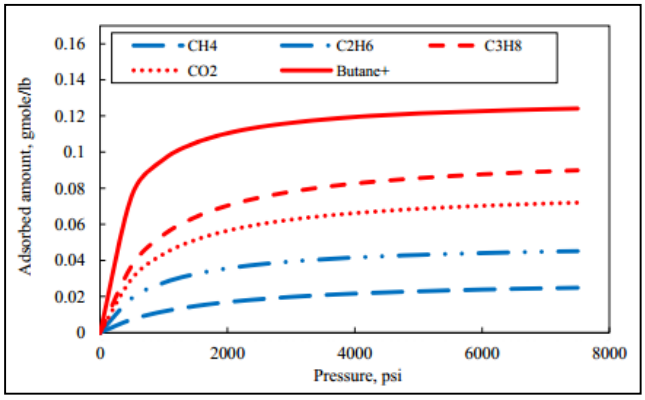

Figure 2- 8 Adsorption Isotherms for different Components
(Haghshenas, 2014)

2.8 Summary

In this chapter, some of the key fundamentals of fluid flow and hydrocarbon storage in liquid rich reservoirs were discussed. These include capillary pressure, diffusion, shift in critical properties and adsorption. Such forces become more significant at nano-scale because of the increased interactions between fluid molecules and the pore walls and amongst fluid molecules themselves. Capillary pressure causes supression in the bubble point pressure. This phenomenun leads to gas being dissolved in oil even below the bulk bubble point pressure, thus decreasing oil density & viscousity, and sustaining Gas Oil Ratio (GOR) for a longer period. Diffusion appeared to be an important phenomenun in gas condensate reservoirs. Confinement was also discussed to cause shift in the critical properties and these shifts are likely to have a drastic impact on hydrocarbon production. Finally, adsorption phenomena was discussed to be a strong function of fluid components' molecular weight and pore configuration. Negligence of adsorption of heavier components, which could be an important storage mechanism of liquids in shale reservoirs, can lead to considerable error in reserve estimation

In the next Chapter, we shall discuss the modifications required in conventional thermodynamics to incorporate capillary pressure.

Chapter 3

Implementation of Capillarity for Tight Pore Reservoirs in AD-GPRS

This chapter discusses the methodology used in this research work to modify conventional thermodynamics in order to incorporate capillary pressure when modelling flow in liquid rich shale reservoirs. The methodology described can be readily implemented in modern reservoir simulator. The chapter begins by offering a detailed account on some of the key thermodynamic concepts and later extends these same concepts towards incorporating capillary pressure in vapor liquid equilibrium computations, so as to offer a better representation of fluid flow in confinement.

3.1 Classical Thermodynamics

Thermodynamics is a branch of physics concerned with heat and temperature and their relation to energy and work, in near-equilibrium systems. Classical thermodynamics describes the bulk behavior of the body and not the microscopic behaviors of the very large numbers of its microscopic constituents, such as molecules (Vidal, 1997). These general constraints are expressed in the four laws of thermodynamics. In the petroleum industry, thermodynamics of phase equilibria attempts to answer "Under given temperature and pressure and mass of components, what are the amounts and composition of phases that result?" (Kovscek, 1996)

3.1.1 Equation of State

At the heart of thermodynamics lies the equation of state, which in simplest terms is a formula describing the interconnection between various macroscopically measurable properties of a system. More specifically, an equation of state is a thermodynamic equation describing the "state of matter under a given set of physical conditions. It is a constitutive equation which provides a mathematical relationship between two or more state functions associated with the matter, such as its temperature, pressure, volume, or internal energy" (Thijssen, 2013).

Equations of state are instrumental in the calculation of Pressure-Volume-Temperature (PVT) behavior of petroleum gas/liquid systems at equilibrium. Reservoir fluids contain a variety of substances of diverse chemical nature that include hydrocarbons and nonhydrocarbons (Ashour, 2011). Hydrocarbons range from methane to substances that may contain 100 carbon atoms. In spite of the complexity of hydrocarbon fluids found in underground reservoirs, equations of state have shown surprising performance in the phase-behavior calculations of these complex fluids (Ashour, 2011).

Since till to date, no single equation of state accurately predicts the properties of all substances under all conditions, a number of equations of state have been developed for gases and liquids, over the course of thermodynamics history. Among the various categories of EOS, the Cubic Equations of State have been used in this work, as they have been widely used and tested for predicting the behavior of hydrocarbon systems (Ashour, 2011) (Kovscek, 1996).

The generalized form of cubic equation of state is shown in equation 3-1 (Kovscek, 1996) (Gmehling, 2012), where each of the four parameters *a*, *b*, *u* and *w*, depend on the actual EOS as shown in Table 3-1.

$$P = \frac{RT}{V-b} - \frac{a}{V^2 + ubV + wb^2} \qquad \textbf{(3- 1)}$$

Here, *R* is the ideal gas constant, *T* is temperature and *V* is molar volume.

Table 3-1 Parameter values for Cubic Equation of State (Kovscek, 1996)

Equation of State	**U**	**W**	**B**	**A**
Van der Waals EOS	0	0	$\frac{RT_c}{8P_c}$	$\frac{27R^2T_c^2}{64P_c}$
Redlich-Kwong EOS (RK)	1	0	$\frac{0.08664RT_C}{P_C}$	$\frac{0.42748R^2T_c^{5/2}}{P_cT^{1/2}}$
Soave Redlich-Kwong EOS (SRK)	1	0	$\frac{0.08664RT_C}{P_C}$	$\frac{0.42748R^2T_c^2}{P_c}\left[1+f_\omega\left(1-T_r^{1/2}\right)\right]^2$ where $f_\omega = 0.48+1.574\omega-0.176\omega^2$
Peng Robinson EOS (PR)	2	-1	$\frac{0.07780RT_c}{P_c}$	$\frac{0.45724R^2T_c^2}{P_c}\left[1+f_\omega\left(1-T_r^{1/2}\right)\right]^2$ where $f_\omega = 0.37464+1.54226\omega-0.2699\omega^2$

In the above table, T_c and P_c are the critical temperature and pressure respectively, ω is the acentric factor and f_ω is the acentric factor function.

When dealing with mixtures, mixing rule (Kwak, 1986) are applied to parameters *a* and *b:*

$$a_v = \sum_i \sum_i y_i y_j \left(a_i a_j\right)^{1/2}\left(1-\bar{k}_{ij}\right) \qquad \textbf{(3- 2)}$$

$$b_v = \sum_i y_i b_i \qquad \textbf{(3- 3)}$$

Here *v* represents the vapor phase. In order to calculate a_l and b_l (where subscript *l* represents the liquid phase) *y* in equations (3-2) and (3-3) will have to be replaced by liquid phase molar compositions of each component, often denoted by *x*. Each equation requires an independent determination of $\bar{k}_{ij}$ or binary interaction coefficients, which are set zero for Vander Waals and RK EOS by definition.

More commonly, equation (3-1) is written in terms of the Compressibility factor *Z* (Kovscek, 1996) (Grguri, 2003):

$$Z^3 - \left(1 + B^* - \mu B^*\right) Z^2 + \left(A^* + \omega B^{*2} - \mu B^* - \mu B^{*2}\right) Z - A^* B^* - wB^{*2} - \omega B^{*3} = 0 \quad \textbf{(3- 4)}$$

Where

$$A^* = \frac{aP}{R^2 T^2} \quad \textbf{(3- 5)}$$

$$B^* = \frac{bP}{RT} \quad \textbf{(3 - 6)}$$

3.1.2 Condition of Equilibrium

One of the most fundamental relationships in thermodynamics is given by equation (3-7) (Firincioglu, 2014):

$$\Delta U^T = \Delta Q - \Delta W + \sum_i^{nc} \mu_i N_i \quad \textbf{(3- 7)}$$

Upon substituting the expression for ΔQ and ΔW **,** and rearranging equation (3-7), we get a fundamental thermodynamic relationship and the definition of Gibbs free energy:

$$dG = Vdp - Sdt + \sum_{i=1}^{nc} \mu_i dN_i \quad \textbf{(3- 8)}$$

Here *G* is Gibbs free energy, V is Volume is m^3 , *dp* is change in pressure in bars, *S* is Entropy in joule/K, *dt* is the change in temperature is *K*, μ is the chemical potential, *N* is the number of moles, *nc* is the total number of components and *i* is the component index.

For a closed system to be in equilibrium, the chemical potential of a component, at a given temperature and pressure condition, must be the same in each phase. The equilibrium condition is thus given by (Firoozabadi, 1999):

$$\mu_i^{\alpha} = \mu_i^{\beta} = \ldots = \mu_i^{N_p}, \qquad i = 1, 2, 3 \ldots, N_c \quad \textbf{(3- 9)}$$

Where α and β are the phases and N_p and N_c are the total number of phases and components respectively.

(Lewis, 1923) proposed the folowing expression for Gibbs free energy:

$$dG_i = RTd \ln f_i \quad \textbf{(3- 10)}$$

Where f_i is the fugacity of component *i.*

Fugacity is often computed from a relationship comprising of a dimensionless variable called 'fugacity coefficient' (Matar, 2009). This is given by:

$$\phi_i = f_i \big/ P \quad \textbf{(3- 11)}$$

Here ϕ_i is the fugacity of component *i* and is computed using the following expression that has been derived using the general form of cubic equation (Kovscek, 1996) (Matar, 2009):

$$\ln \hat{\phi}_i = \frac{b_i}{b}(Z-1) - \ln\left(Z - B^*\right) + \frac{A^*}{B^*\sqrt{\mu^2 - 4\omega}}\left(\frac{b_i}{b} - \delta_i\right)\ln\frac{2Z + B^*\left(\mu + \sqrt{\mu^2 - 4\omega}\right)}{2Z + B^*\left(\mu - \sqrt{\mu^2 - 4\omega}\right)} \quad \textbf{(3- 12)}$$

Where,

$$\frac{b_i}{b} = \frac{T_{ci}/P_{ci}}{\sum x_j T_{cj}/P_{cj}} \quad \textbf{(3- 13)}$$

$$\delta_i = \frac{2a_i^{1/2}}{a}\sum_j x_j a_j^{1/2}\left(1 - \bar{k}_{ij}\right) \quad \textbf{(3- 14)}$$

Here A^* and B^* are given by equations (3-5) and (3-6).

At an equilibrium condition at constant temperature and pressure, we know $dG_i = 0$ and $dP = dt = 0$. Substituting this in equation (3-8) we get:

$$G_i = \mu_i \quad \textbf{(3- 15)}$$

For the fugacity of component *i* then, it must hold that

$$dG_i = d\mu_i = RTd \ln f_i \quad \textbf{(3- 16)}$$

and the equality of the chemical potential translates into an equality of fugacity (Kovscek, 1996). Thus, at equilibrium, we have:

$$\mu_i^{\alpha} = \mu_i^{\beta} = ... = \mu_i^{N_p} \Rightarrow \quad f_i^{\alpha} = f_i^{\beta} = ... = f_i^{N_p} \qquad i = 1, 2, 3..., N_c \tag{3- 17}$$

3.1.3 Vapor Liquid Equilibrium / Flash Computatution

Using flash one can obtain the equilibrium composition of two co-existing phases and solve for bubble and dew point pressures. The general flash routine that AD-GPRS[1] follows is outlined as under. This method also closely follows the algorithm illustrated by Kovscek (1996). A simplified representation of flash is illustrated in the following flow chart:

[1] AD-GPRS which stands for Automatic Differentiation General Purpose Research Simulator, is Stanford University's in-house reservoir simulator.

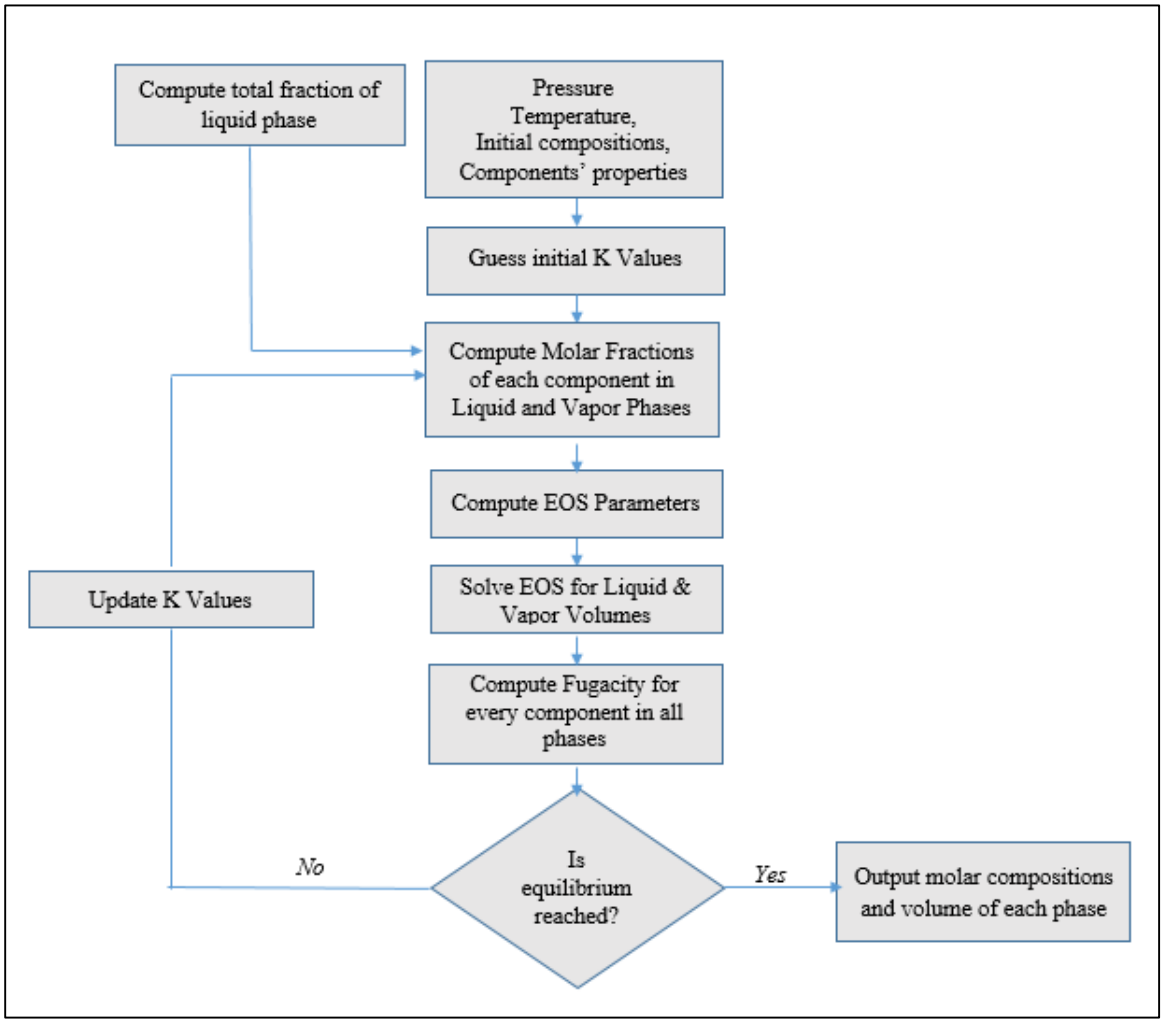

Figure 3-1 Conventional Vapor Liquid Equilibrium Workflow

1. Guess K-Values

The first step to make an initial guess for *K-values*, where *K* is the equilibrium ratio given by $K = y_i / x_i$ and x_i and y_i are the liquid and gaseous molar fractions of component i. This initial guess can be computed using Wilson's Equation (Wilson, 1969):

$$K_i = \frac{y_i}{x_i} = \frac{P_{ci}}{P} \exp\left[5.37\left(1 + w_i\right)\left(1 - \frac{T_{ci}}{T}\right)\right] \qquad \textbf{(3- 18)}$$

Here, P_{ci} and T_{ci} are the critical pressure and temperature of a component with index *i*. w_i is the accentric factor of the component.

2. Flash

The mixture is then flashed in order to determine the vapor and liquid compositions. For two phases, a mass balance on 1 mole of mixture yeilds the following:

$$z_i = x_i l + y_i (1-l) \qquad \textbf{(3- 19)}$$

Here z_i is the overall composition of a component in the system and l is the mole fraction of the mixture that is present in liquid phase. Plugging $K = y_i / x_i$ into equation (3-19), we get expressions for the liquid and gaseous molar fractions for each components as follows:

$$x_i = \frac{z_i}{l + (1-l) K_i} \qquad \textbf{(3- 20)}$$

$$y_i = \frac{K_i z_i}{l + (1-l) K_i} \qquad \textbf{(3-21)}$$

Using the fact that the sum of all mole fractions in each phase must be one, we can combine equations (3-20) and (3-21) to yeild:

$$f(l) = \sum_i^{nc} \frac{z_i (1-K_i)}{K_i + (1-K_i) l} = 0 \qquad \textbf{(3- 22)}$$

Equation (3-22) is called the Rachford Rice Equation (Rachford, 1952) and can be iteratively solved to obtain l (the unknown) liquid fraction. The converged value of l tells whether the system is in single vapor phase ($l < 0$), two phases ($0 \le l \le 1$) or single liquid phase ($l > 1$). Additionally, once l is known, equations (3-20) and (3-21) can be used to obtain the liquid and vapor compositions of each component in the system. Mixed Newton/Bisection method is often used to solve for l.

3. Computation of EOS Parameters

Phase molar compositions thus otained can be substituted in equations (3-2) and (3-3) to obtain respective EOS paramemeter for each phase, that is, a_v, a_l, b_v and b_l.

4. Solving EOS for Liquid and Vapor Volumes

If there are two phases present in the system, the EOS will be solved twice (one for each phase) using its respective phase EOS parameters. Each soulation gives the volume of its respective phase. At given P and T, the compressibility factor Z is computed for each phase (that is Z^v and Z^l) using equation (3-4). Note that inorder to do that, A^* and B^* in equations (3-5) and (3-6) too are seperatedly computed for each phase. For instance, A_v^* uses a_v and A_l^* uses a_l.

The cubic equation returns three roots of Z each time it is solved and the right root is selected on the basis of whichever minimizes the Gibbs energy the most. The sign of ΔG determines the physical root of Z. That is if,

$$\Delta G > 0 \quad \Rightarrow \quad Z^v \text{ is the physical root}$$

$$\Delta G < 0 \quad \Rightarrow \quad Z^l \text{ is the physical root}$$

5. Computation of Fugasities

Once liquid and vapor volumes are computed, we use equation (3-12) to compute fugasity coefficients for every component i and equation (3-11) to compute the corresponding fugacities.

6. Convergence-

The system is in equilibrium when the following is true for all components:

$$\hat{f}_i^l = \hat{f}_i^v \quad , \qquad i = 1, 2, ...N_c$$

Numerically, this is equivalent to

$$\left| \frac{\hat{f}_i^l}{\hat{f}_i^v} - 1 \right| < \varepsilon \qquad \textbf{(3- 23)}$$

Here ε is a small number, usually in the range of 10^{-4} to 10^{-6} .

7. Updating K Values-

Each time a new K value is calculated, the system is checked for equilibrium. This can be done using Successive Substitution (SSI) method. Thus K can be computed as:

$$\left(K_i\right)^{k+1} = \left(\frac{\hat{f}_i^l}{\hat{f}_i^v} K_i \right)^k \qquad \textbf{(3- 24)}$$

New values of l can thus be generated by computed K values and by solving equation (3-22).

3.2 Modification of Flash to Incorporate Capillary Pressure in Tight Pores

Conventional flash involves the computation of all EOS parameters & fugacity for each phase at a single pressure (Nojabaei, 2012). That is:

$$\hat{f}_i^l = \hat{f}_i^l\left(P, V^l, T, x_1, x_2, \ldots\right) \quad , \quad \hat{f}_i^v = \hat{f}_i^v\left(P, V^v, T, x_1, x_2, \ldots\right)$$

This works well for conventional reservoirs, but for tight reservoirs each phase has to be treated against its own respective phase pressure. Therefore, fugacity is now defined by the following-

$$\hat{f}_i^l = \hat{f}_i^l\left(P^l, V^l, T, x_1, x_2, \ldots\right) \quad , \quad \hat{f}_i^v = \hat{f}_i^v\left(P^v, V^v, T, x_1, x_2, \ldots\right)$$

When the capillary forces are considered, the phase pressures are no longer equal and the difference is given by Laplace equation which is as follows:

$$P_{cap} = P_g - P_l = \frac{2\sigma\cos\theta}{r} \qquad \textbf{(3- 25)}$$

Here, P_{cap} is the Capillary Pressure, P_g and P_l are the gas (vapor) phase and liquid (oil) phase pressures, r is the pore radius, θ is the wettability angle and σ is the Interfacial tension. In this work we will treat the wettability angle to be 180^o or in other words consider the reservoir to be oil wet, which in many cases, such as Bakken shale reservoir, is a valid assumption (Fine, 2009). Therefore, equation (3-25) gets simplified to the following:

$$P_{cap} = \frac{2\sigma}{r} \qquad \textbf{(3- 26)}$$

There are several correlations and methods to calculate the interfacial tension (IFT). According to Ayirala (Ayirala, 2006), the most important among these models are the Parachor model (Macleod, 1923) (Sudgen, 1924), the corresponding states theory (Brock, 1955), thermodynamic correlations (Clever,1963), and the gradient theory (Carey, 1979). In this work, Macleod-Sugden (MS) formulation has been used to calculate IFT because it is most widely used in the petroleum industry due to its simplicity (Ayirala, 2006). Equation (3-27) presents the MS formulation:

$$\sigma = \left[\sum_i \gamma_i\left(x_i\rho^L - y_i\rho^V\right)\right]^4 \qquad \textbf{(3- 27)}$$

Here γ_i is components' Parachor value and ρ^L and ρ^V are liquid and vapor densities respectively. Thus, interfacial tension is a function of changes in densities, compositions

and Parachor, and becomes zero at the critical point where phase properties start approaching each other.

The flash flow chart presented in Figure 3-1 can thus be modified as illustrated in Figure 3-2 to incorporate capillary pressure. Here, the red boxed parameters get influenced by capillary pressure, which in turn influences the whole flash. A more detailed illustration of the modified VLE algorithm is given in Appendix A. Similar modifications in the VLE to accommodate capillary pressure have been done by Firincioglu (2014) and Nojabaei (2012), previously.

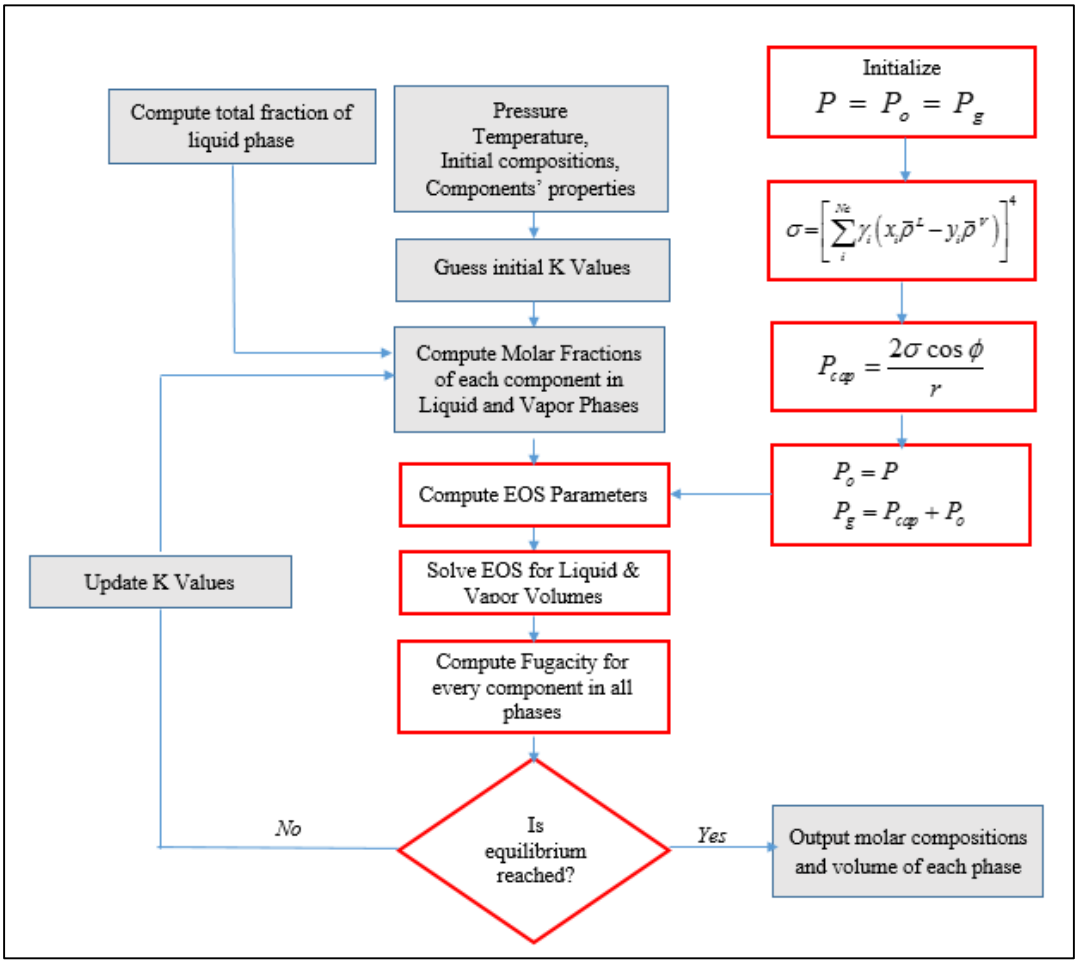

Figure 3-2 Modified Vapor Liquid Workflow to Incorporate Capillary Pressure

3.3 Stability Test using Gibbs Free Energy approach

It has been shown by Wang (2013) that standard stability test based on tangent plane distance analysis can be extended to consider capillarity effect. Michelsen (1982) showed that equation (3-28) holds true if the original system is stable:

$$\sum_{i}^{m} y_i \left[\ln f_i(y) - \ln(z) \right] \geq 0 \qquad \textbf{(3- 28)}$$

where, $f_i(y)$ is the fugacity of the incipient phase of component *i*, while $f_i(z)$ is its fugacity in the original system. Here the original phase is liquid and the incipient phase is vapor. If the original phase were vapor, the incipient must have been liquid.

Considering the definition of fugacity:

$$f_i(z) = z_i \phi_i(z) P^L \qquad \textbf{(3- 29)}$$

$$f_i(y) = z_i \phi_i(z) P^V \qquad \textbf{(3- 30)}$$

where ϕ_i is the fugacity coefficient of component *i*, we can substitute equations (3-29) and (3-30) in equation (3-28) to get the following expression:

$$\sum_{i}^{M} y_i \left[\ln\left(y_i \phi_i(y) P^V \right) - \ln\left(z_i \phi(z) P^L \right) \right] \qquad \textbf{(3- 31)}$$

Some rearrangement of equation (3-31) and (3-28) can yield the following:

$$\sum_{i}^{M} y_i \left[\ln y_i + \ln \phi(y) - \ln z_i - \ln \phi(z) + \left(\ln P^V - \ln P^L \right) \right] \geq 0 \qquad \textbf{(3- 32)}$$

Thus using this approach Wang (2013) showed that the capillary term $\left(\ln P^V - \ln P^L \right)$ is naturally incorporated in the equilibrium test.

3.3 Summary

In this chapter, we presented a detailed background of thermodynamics related to fluid flow in porous media and how it can be modified to incorporate capillary pressure that becomes significant in tight pores, using a methodology that can be readily used in modern compositional simulators.

In the next chapter, this methodology will be used to decipher the influence of capillary pressure on fluid phase behavior in tight pore reservoirs.

Chapter 4

Investigation on the Influence of Capillarity on Confined Fluid Behavior

Capillary pressure can have considerable impact on the overall recovery of hydrocarbons (Alharthy, 2013) (Firincioglu, 2014) (Nojabaei, 2014). This chapter investigates the changes in fluid phase behavior that can result due to the influence of capillary forces that arise in tight pores. A secondary goal of this work is to compare the results obtained using AD-GPRS with published literature where appropriate. We begin our study with simple binary mixtures, followed by a more realistic Bakken fluid.

4.1 Investigation on the Influence of Capillary Pressure using Binary Mixtures

This section follows the work of Nojabaei (2012), however unlike the author, we extented a fully compositional simulator (AD-GPRS[2]) to model the impact of capillarity on phase behavior as a function of pore radius.

We first investigated the impact of capillary pressure on bubble point by varying the pore size, using a binary mixture composed of 30% C1 and 70% C6. Figure 4-1 illustrates that small pore radii can cause significant reduction in the bubble point pressure. For this mixture, the influence of capillary pressure fades away as the pore size approaches 100 nm. The phase envelope calculations use Peng Robinson Equation of State (EOS) discussed in the previous section. The impact of capillary pressure on dew points is not shown here. Based on published literature (Nojabaei, 2012) (Teklu, 2014), dew points also get shifted but often in magnitudes that are lesser than the bubble point shifts. Capillary pressure makes dew point appear sooner or at relatively higher reservoir pressures (Alharthy, 2013).

[2] AD-GPRS stands for Automatic Differentiation General Purpose Research Simulator and is Stanford University's in-house reservoir simulator.

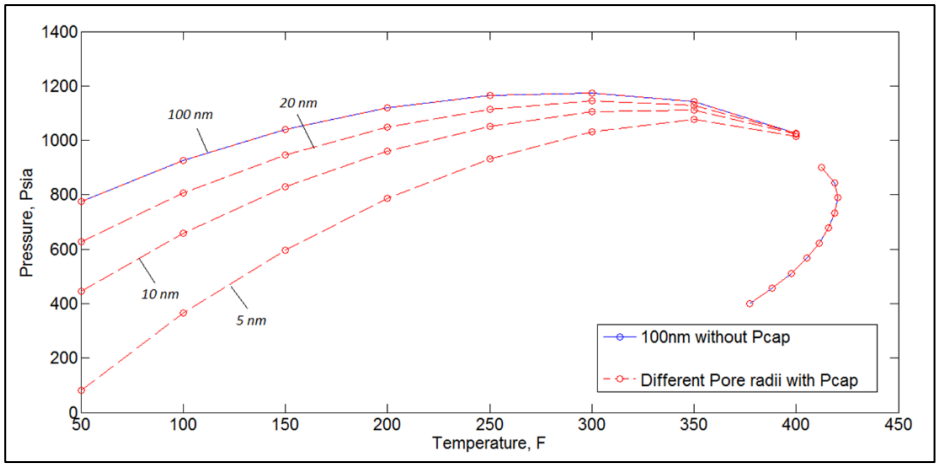

Figure 4- 1 Impact of Pore Radius on Bubble Point Suppression

Next the pore size was fixed to 10 nm and the influence of varying compositions of the binary mixture on bubble point supression was studied. The amount of methane was varied in the binary mixture comprising of $C_1 - C_6$. Figure 4-2 shows the phase envelopes both with and without capillary pressure. With the increase in the percentage of the heavier compenent C_6 in the system, the critical pressure positions' shift. This influences the strength of capillary pressure, which in turn gets translated into higher bubble point suppression. This is because higher bubble point pressures reduce the density differences between liquid and vapor (Nojabaei, 2012) and thus suppress the impact of capillarity.

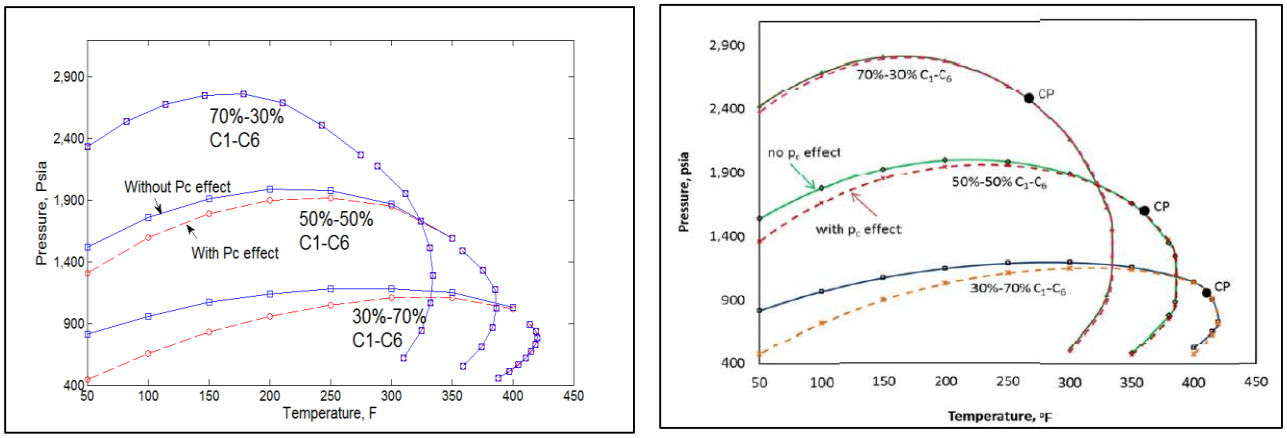

Figure 4- 2 Influence of varying composition of C1-C6 on capillary pressure's influence.
Left: AD-GPRS**, Right:** (Nojabaei, 2012)

Since capillary pressure is a function of vapor and liquid phase densities, the changes in densities at various locations of the phase envelope was determined next. Figure 4-3 shows the phase envelope of a binary mixture composed of 70% C_1 and 30% C_6. Point D and F marked on the envelope are close to the bubble and dew point pressures respectively, while Point E lies in between them. The percentage density change of each phase with and without capillary pressure is shown in Figure 4-4. The solid lines represent percentage density difference with and without capillarity for oil phase at each of the marked locations, while the dotted lines represent vapor phase. The highest density difference achieved in oil phase near the bubble point at a pore radius of 2.857 nm is approximately 7%. The highest density difference achieved in the vapor phase is around 5% and is near the dew point. Since capillarity is a function of interfacial tension, which is in turn is a function of the differences in densities of both the phases, it can be seen that oil and gas phase densities differ the most from each other at point D, which is close to the bubble point region. This explains why the highest impact of capillary pressure is in the bubble point region.

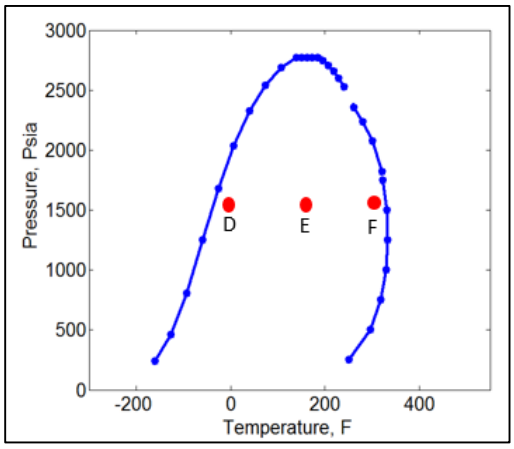

Figure 4- 3 Points indicating various positions in the phase envelope of 70% C1- 30% C6

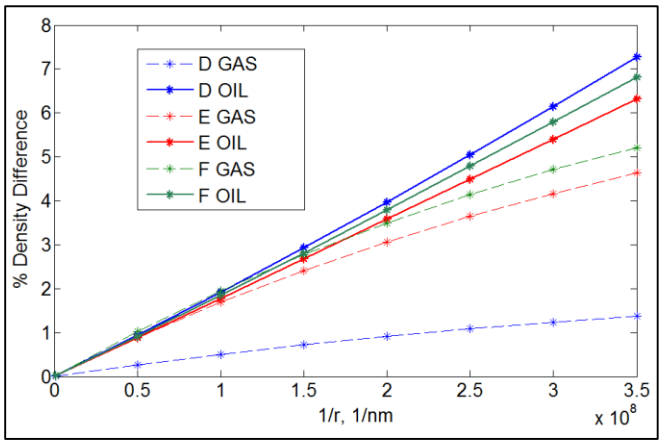

Figure 4- 4 Percentage density differences caused by capillary pressure in liquid and vapor phases at the positions shown in Figure 4-3

4.2 Investigation of the Influence of Capillary Pressure using Bakken Fluid Composition

From the results obtained using binary mixture fluid compositions, it can be concluded that capillary pressure suppresses bubble point and causes the fluid densities to change. Further on, magnitude of capillary pressure is a function of pore radius, fluid composition and the pressure & temperature conditions. We next extended this study to more realistic fluid composition obtained from Bakken. Figure 4-5 shows the phase envelope of a Bakken fluid sample bearing the composition given in Table 4-1. More information on fluid properties can be obtained from Nojabaei (2012).

Table 4 - 1 Composition of Bakken fluid sample (Nojabaei, 2012)

Component	C1	C2	C3	C4	C5-6	C7-12	C13-21	C22-80
Molar Fraction	0.36736	0.14885	0.09334	0.05751	0.06406	0.15854	0.0733	0.03704

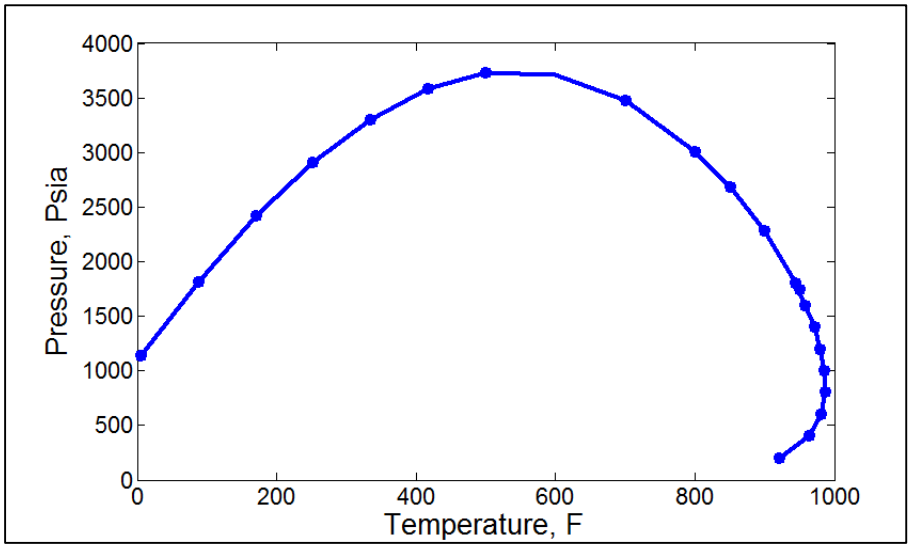

Figure 4- 5 Phase Envelope of Bakken Fluid Sample

A typical tight reservoir such as Bakken has a pore radius ranging from 10 nm to 50 nm (Wang, 2013). Therefore, capillary pressure should be of influence its fluid's phase behavioral properties. Figure 4-6 shows the suppression of bubble point pressure of Bakken fluid phase envelope at a pore radius of 10 nm. This suppression can lead to considerable deviation of fluid flow properties from its respective unconfined state. Additionally, suppression in Bakken fluid's bubble point starts fading away quickly as the pore radius approaches 100 nm.

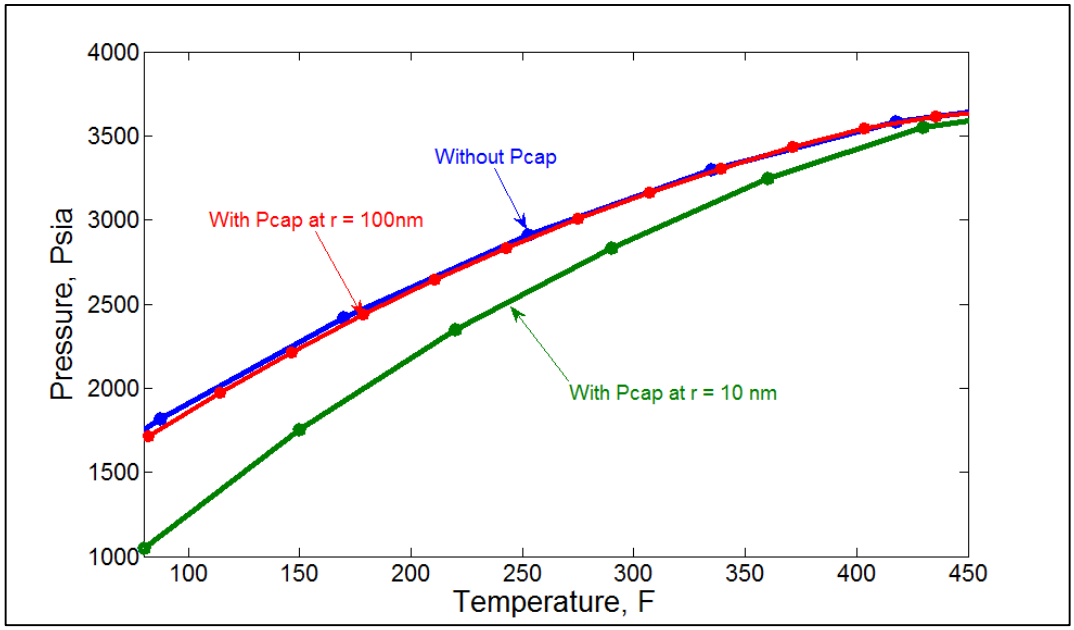

Figure 4- 6 Bakken fluid phase envelope bubble point suppression under the influence of capillarity

As was discussed in Chapter 2, the suppression of bubble point pressure leads to the retention of gas in oil for a longer time as the pressure is reduced, and will density and viscosity of oil. This led to the investigation of the impact of pore radius on Bakken fluid density. Figure 4-7 shows reduction in oil density as the pore radius increases and the reservoir pressure decreases. This indicates that capillarity becomes more influential at lower reservoir pressures. Oil viscosity displays a similar trend, as shown in Figure 4-8. Gas density and viscosity on the other hand show an increase when pores become tighter, as shown in Figures 4-9 and 4-10. Each of the results have been matched against the results obtained by Nojabaei (2014). The results only display densities and viscosities till the bubble point pressures as the capillary pressure becomes zero above that. Owing to the uncertainty in interfacial tension (IFT) calculations and Macleod & Sugden correlation's tendency to under-predict IFT (Ayirala, 2006), cases were included where IFT was multiplied by a factor of 3. All of cases obtained by Nojabaei (2014) that are shown below have IFT multiplied by 3. The final figure, Figure 4-11, shows the density of oil as a function of pore radius when the reference pressure is change from oil phase pressure to gas phase pressure, that is, $P_o = P_g - P_{cap}$ instead of $P_g = P_o + P_{cap}$.

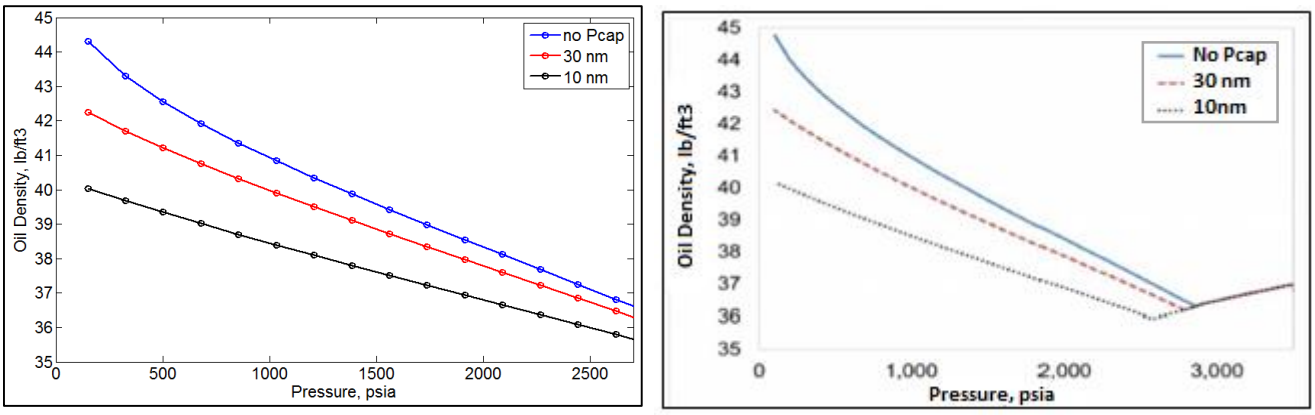

Figure 4- 7 Bakken oil density as a function of pore radius and oil phase (reservoir) pressure.
Left: AD-GPRS, **Right:** (Nojabaei, 2014)

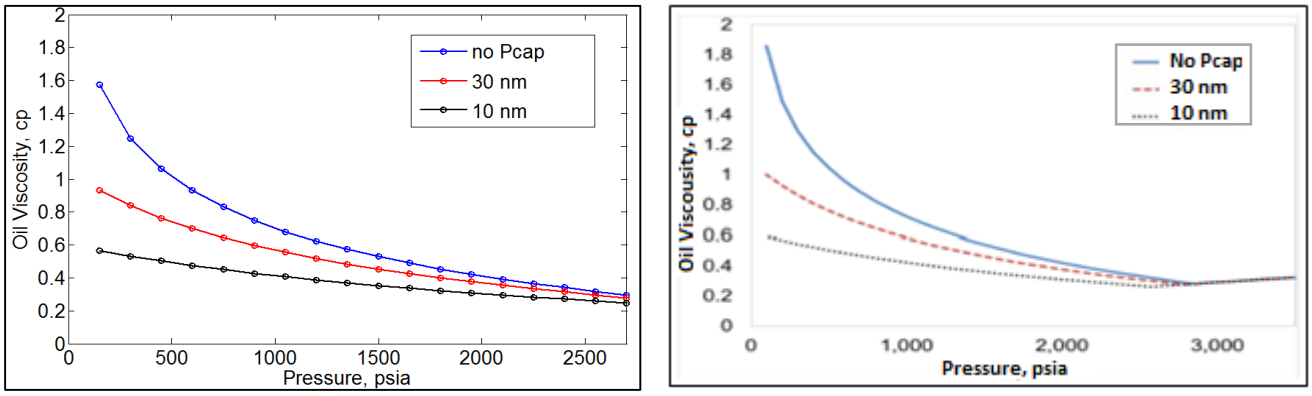

Figure 4- 8 Bakken oil viscosity as a function of pore radius and oil phase (reservoir) pressure
Left: AD-GPRS, **Right:** (Nojabaei, 2014)

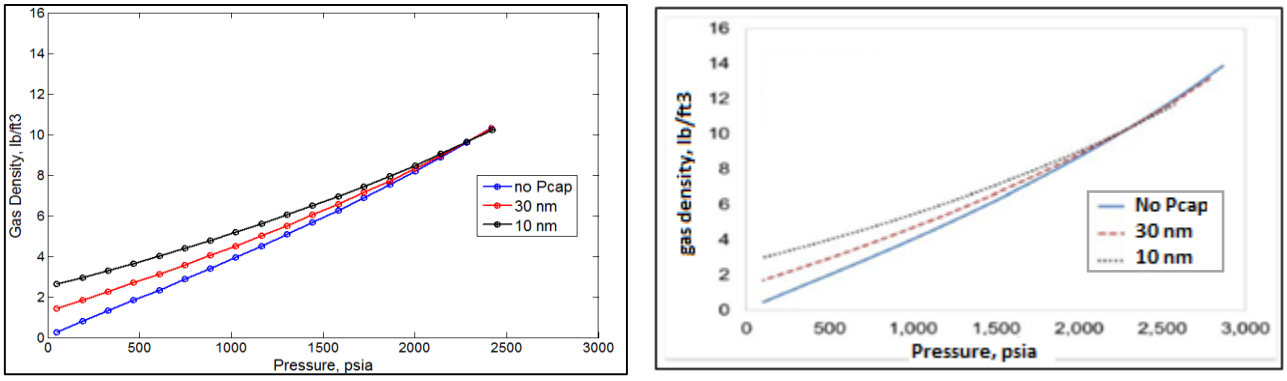

Figure 4- 9 Bakken gas density as a function of pore radius and oil phase (reservoir) pressure
Left: AD-GPRS, **Right:** (Nojabaei, 2014)

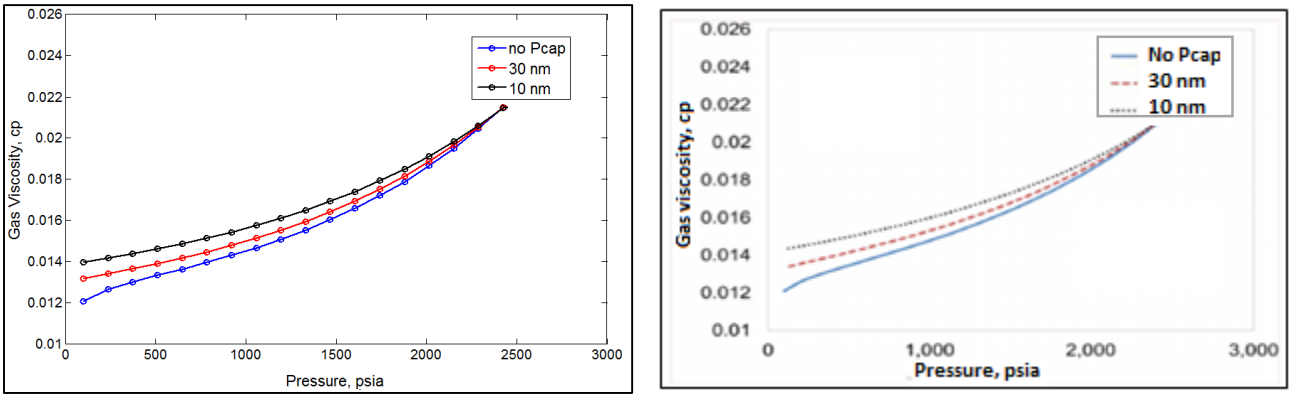

Figure 4- 10 Bakken gas viscosity as a function of pore radius and oil phase (reservoir) pressure
Left: AD-GPRS, **Right:** (Nojabaei, 2014)

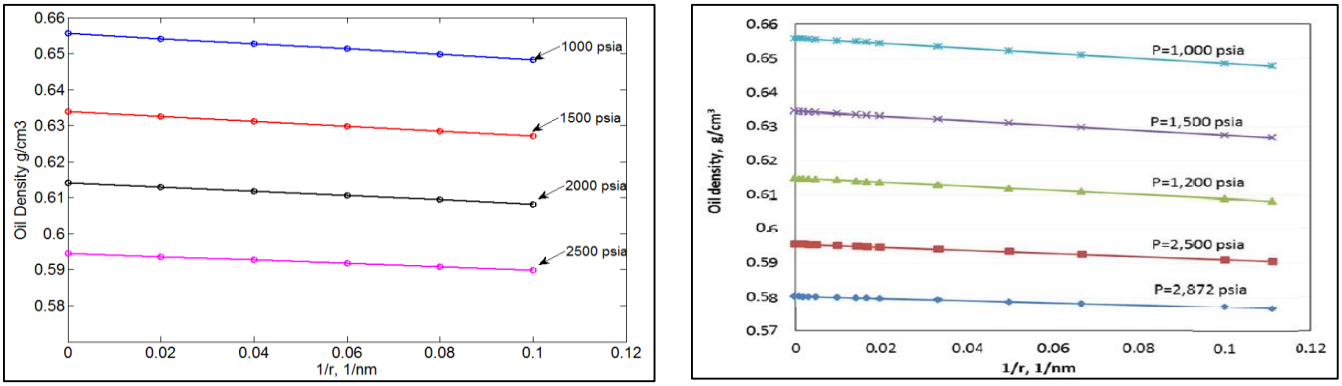

Figure 4- 11 Bakken oil density as a function of pore radius and gas phase pressure
Left: AD-GPRS, **Right:** (Nojabaei, 2012)

4.3 Summary

In this chapter, changes in fluid phase behavior due to the influence of capillary forces in tight pores, were investigated. Capillary pressure can cause significant reduction in the bubble point pressure, and oil density and viscosity. Gas density and viscosity were shown to have increased on the contrary. It was also shown that the magnitude of capillary pressure depends on pore size, reservoir pressure and fluid composition. For the specific Bakken fluid sample under investigation, capillary pressure influenced fluid phase behavior for pore radii less than 100 nm.

An important goal of this chapter was to compare the results obtained using AD-GPRS with published literature where appropriate, by extending a compositional simulator to incorporate capillary pressure. This and Chapter 5 were used to prepare ground for the work on more realistic reservoir models that will be presented in Chapter 6.

Chapter 5

Testing Implementation of Capillarity for Tight Pores in AD-GPRS with Production

Incoporating capillary pressure and the impact of confinement on the performance of liquid rich shale reservoirs in fully compositional reservoir simulators is a relatively novel research direction and so current commercial simulators are not equipped with this capability. Therefore, after having matched fluid phase behavior results with published literature, capillary pressure formulation in AD-GPRS was put to further testing in the presence of sources/wells in the system.

5.1 Test Case 1

Testing the formulation with Source but no Capillary Pressure

The first case developed for this purpose has a single source in the system and capillary pressure in modified AD-GPRS has been set to zero. This effect can be achieved by setting pore radii in all the grid blocks to very large values. The purpose of setting up this case was to test if the modified version of AD-GPRS was performing adequately in the presence of a source, when capillary pressure's influence is absent. A similar case was developed using Schlumberger's commercial simulator Eclipse (E 300, 2013.2). Figure 5-1 shows the results of daily production rates obtained from both the simulators agree well.

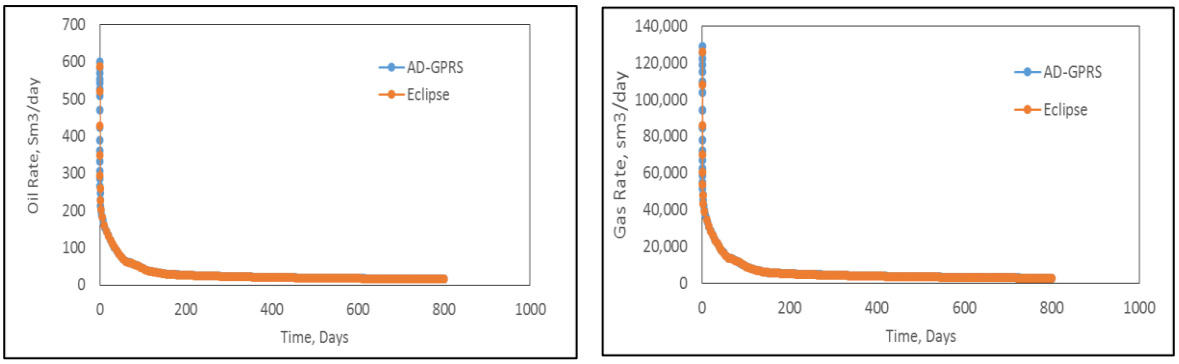

Figure 5 - 1 Comparison of Eclipse and modified AD-GPRS, in the presence of source and with capillary pressure set to zero in AD-GPRS

5.2 Test Case 2

Testing Formulation under the Influence of Capillary Pressure but no Source

Next, all wells in the reservoir were removed so that a mass balance test could be done. The purpose of setting up this case was to test if despite the presence of capillary pressure in the system, the properties of all the blocks where consistent and equal, given that there is no source in the system. A simple case of three blocks was developed and the properties of all the blocks after 200 days of simulation were noted. These were found to be the same in all the grid blocks.

5.3 Test Case 3

Testing Implementation under the influence of both Source and Capillary Pressure

Finally, both the source and capillary pressure were set functional in the system and tests cases were developed both above and below the bubble point of the system. Using Figure 4-6**,** we know that the suppressed bubble point pressure of Bakken fluid sample under the influence of capillary pressure at a pore radius of 10 nm is around ~2300 psia at reservoir temperature of 240 F. The first case constructed was set at a reservoir pressure of 5000 psia and a flowing bottom hole pressure of 3500 psia, both of which are way above the bubble point. Figure 5-2 shows that just as expected, since reservoir pressure bears only single oil phase above the bubble point pressure, the gas rate at reservoir condition is zero, while oil rates shows no difference with and without capillary pressure. Figure 5-3 shows the results for the case when the reservoir and flowing bottom hole pressure are set to 2000 psia and 100 psia respectively, which are below the bubble point. Under the influence of capillary pressure, the oil rates show an increase while gas rates show a decrease. Similar trends, that is, of oil rate increasing and gas rate decreasing have been obtained by various other authors (Wang, 2013) (Firincioglu, 2014).

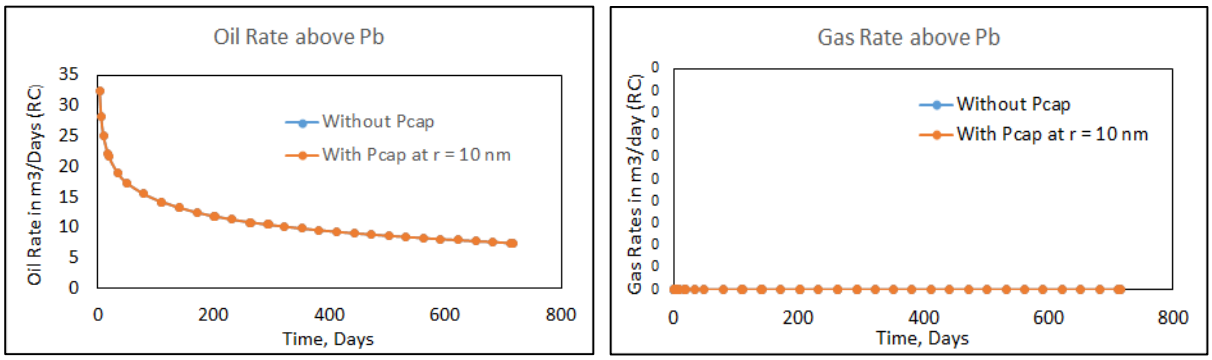

5 – 2 Daily Production rates at reservoir conditions above the bubble point pressure

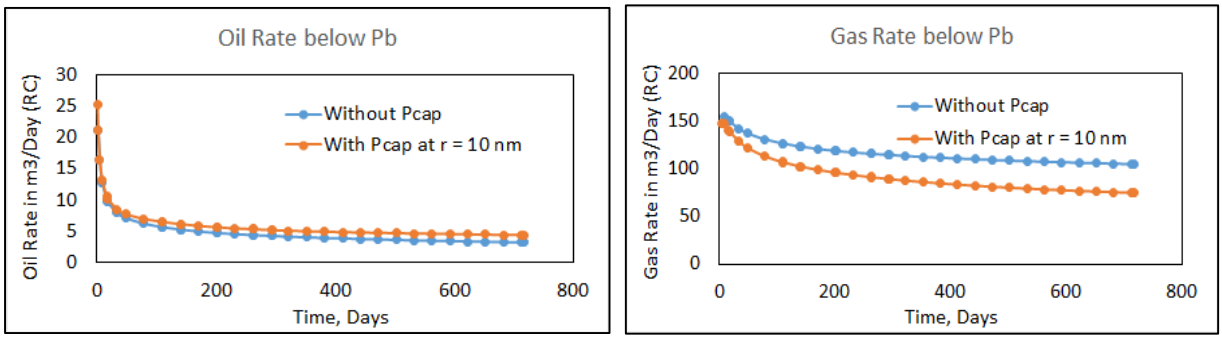

5 - 3 Daily Production rates at reservoir conditions below the bubble point pressure

5.4 Summary

This chapter illustrated the tests done on capillary pressure foumulation in AD-GPRS in the presence of sources/wells. After obtaining successful results in this Chapter and comparisons illustrated in Chapter 4, the impact of confinement on realistic reservoirs scenarios was investigated next.

Chapter 6

Influence of Capillarity and Critical Properties Shifts due to Confinement in Realistic Reservoir Scenarios

Investigation on the influence of capillary forces on fluid phase behavior indicated that these can have a considerable impact on reservoir performance. After having tested the formulation in a variety of ways, different cases were developed to analyze the magnitude of this influence in realistic reservoir systems .This chapter highlights the impact of pore size distribution, variation in fluid composition and alteration of critical properties as a result of confinement, on daily production and over all recovery of hydrocarbon.

6.1 Reservoir Model Set-up

All the cases in the upcoming sections use the reservoir set up depicted in Figure 6-1, with slight modifications to serve their purposes. A single porosity reservoir model bearing 10 fractures and a single horizontal well was constructed. Reservoir and well properties have been listed in Table 6-1. Pore radii in fractures grid blocks were set to very high values so as to avoid capillarity's influence in them.

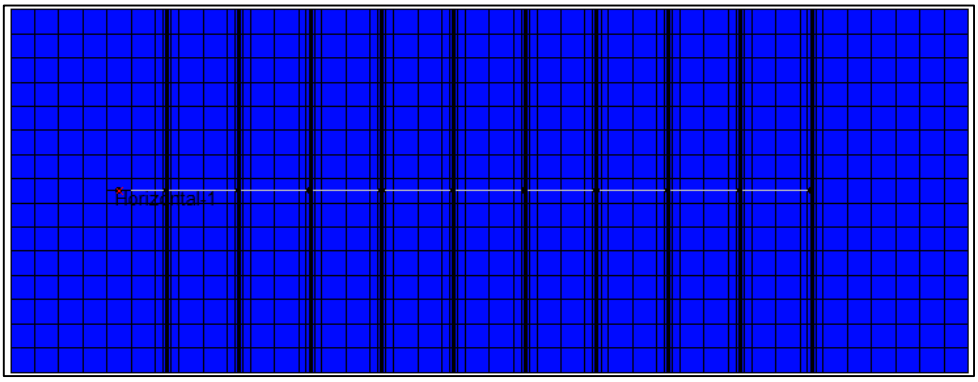

Figure 6 - 1 Reservoir model set up to investigate the influence of capillary pressure on hydrocarbon recovery (image obtained from CMG GEM 2013.11)

Table 6 - 1 Reservoir and Well properties

Number of Grid Blocks	1500 (100 x 15 x 1)
Reservoir Depth	6000 ft
Reservoir Pressure	4200 psi
Reservoir Thickness	100 ft
Reservoir Temperature	240 F
Matrix Permeability	0.01 md
Matrix Porosity	0.05
Fracture Width	2 ft
Fracture Permeability	2.25 md
Fracture Porosity	0.5

6.2 Impact of Pore Radius on Hydrocarbon Production and Recovery

Since oil density and viscosity decrease, while gas density and viscosity increase with the reduction in pore radius based on the findings of Chapter 4, oil production should consequently increase as the pores become tighter, while gas production should decrease. In order to study this, two cases were set up using Bakken fluid system.

6.2.1 Reservoir Conditions above the Bubble Point Pressure

In the first case the initial reservoir pressure was set to 4200 psia which has been cited as being close to Bakken's (wherefrom the sample was collected) current reservoir pressure (Alharthy, 2013) (Nojabaei, 2014), while FBHP was set to 500 psia. Since Figure 4-6 had shown that the bubble point pressure can vary from its original unconfined value of ~2700 psia to values well below it when tighter pore radii cause bubble point pressure suppression, these initial conditions are above the bubble point pressure of Bakken fluid system. Figures 6-2 and 6-3 show that the daily and cumulative production at reservoir conditions do not change significantly as a single well producing at a low FBHP is only able to deplete a few reservoir blocks below the bubble point pressure. Difference in cumulative Oil production at a pore radius of 13 nm from its original unconfined behavior is only ~2% after running the simulation for nearly 6 years, while the difference in gas production is 6.35%. Under confinement oil showed a minor increase while gas production dropped. Even though capillary pressure results in the delay of gas evolution from oil and thus reduces oil density and viscosity, Figures 4-7 to 4-10 show that this reduction gets more and more influential as the reservoir pressure drops to lower values. Thus at conditions that are way above the bubble point pressure, the influence of pore radii and subsequently the capillary pressure is zero.

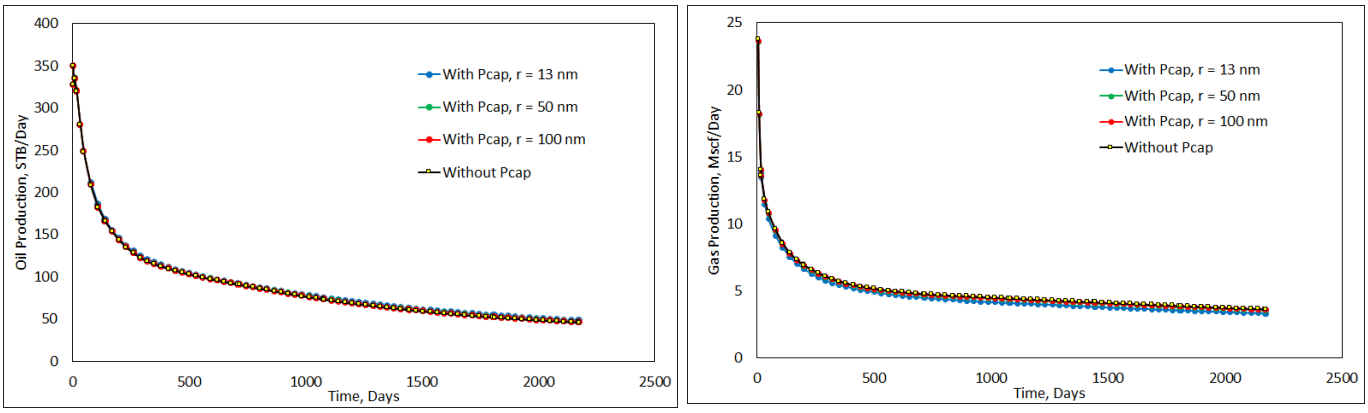

Figure 6 - 2 Daily production rates with reservoir pressure set above P_b of Bakken fluid system at various pore radii

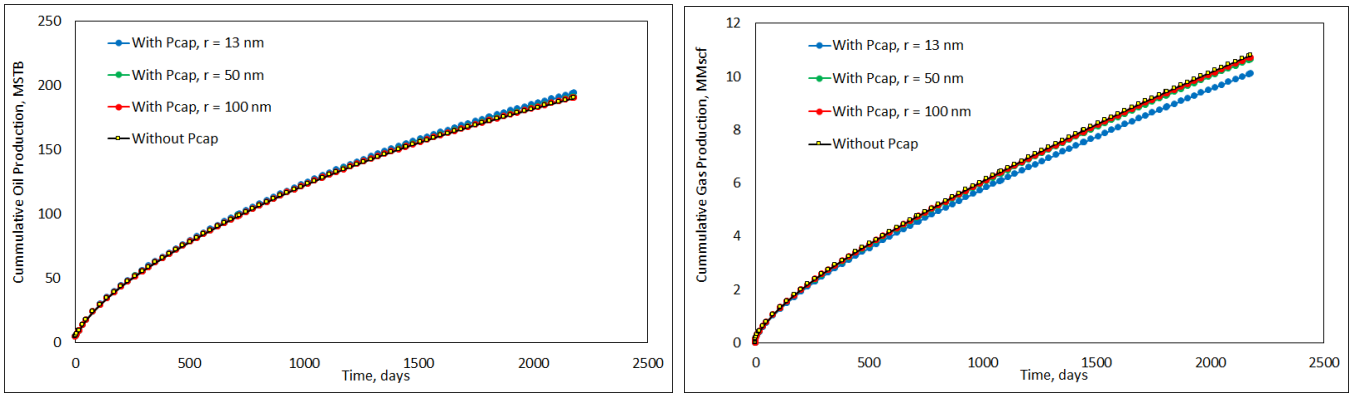

Figure 6 - 3 Cumulative production with reservoir pressure set above P_b of Bakken fluid system at various pore radii

6.2.2 Reservoir Conditions below the Bubble Point Pressure

We next developed a situation that depicts the reservoir pressure of Bakken having fallen below its fluid system's bubble point pressure. The initial reservoir pressure was lowered to 2000 psia, which is well below Bakken fluid's bubble point pressure, and the FBHP set to 100 psia. Figures from 6-4 to 6-6 show that at these lower reservoir pressures, pore radii and subsequently the bubble point pressure has significant influence on hydrocarbon daily production and recovery. At such low pressures, difference in cummulative oil production after ~6 years was found to be 33.2% and while in cumulative gas production to be 15.6%. Also note that just as was depicted by Figure 4-6 that bubble point suppression approaches nearly zero at pore raddii greater than 100nm. Similar trend can be shown in production where difference in cumulative production with and without capillarity approaches zero as

the pore size increases to 100 nm. Since a typical shale field has a high well density, this study can be extended to an interesting field optimization analysis. Depending on the reservoir pressure decline rate and the minimum abandoment pressure, the influence of capillary pressure can be optimized to the operators' advantage.

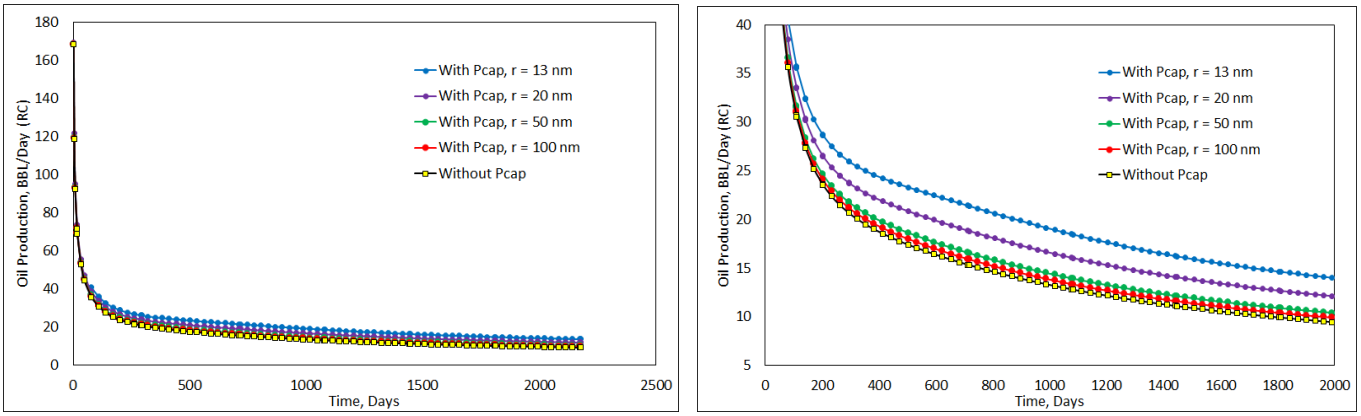

Figure 6 - 4 Left: Daily Oil production with reservoir pressure set below P_b of Bakken fluid system at various pore radii **Right:** Zoomed-in version of the figure on left

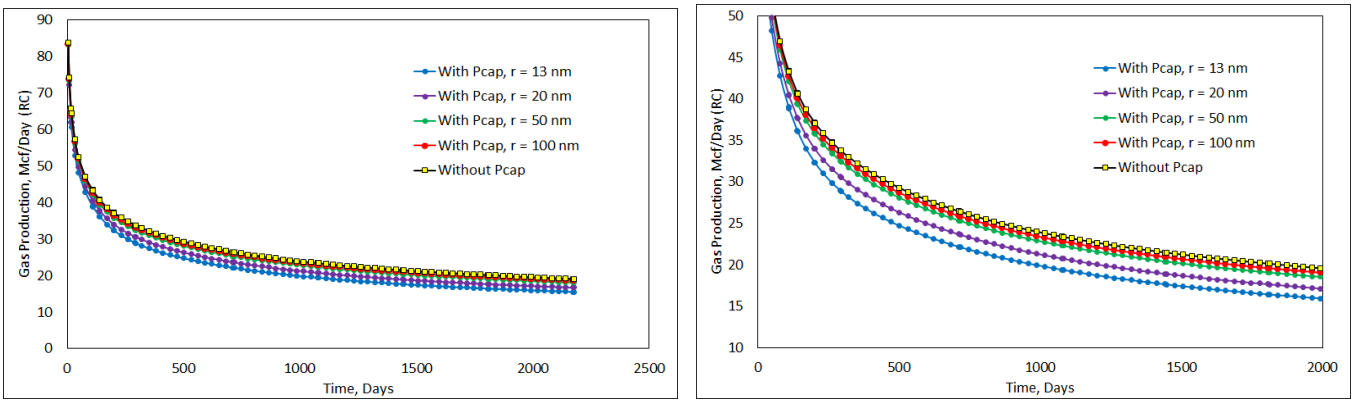

Figure 6 - 5 Left: Daily Gas production with reservoir pressure set below P_b of Bakken fluid system at various pore radii **Right:** Zoomed-in version of the figure on left

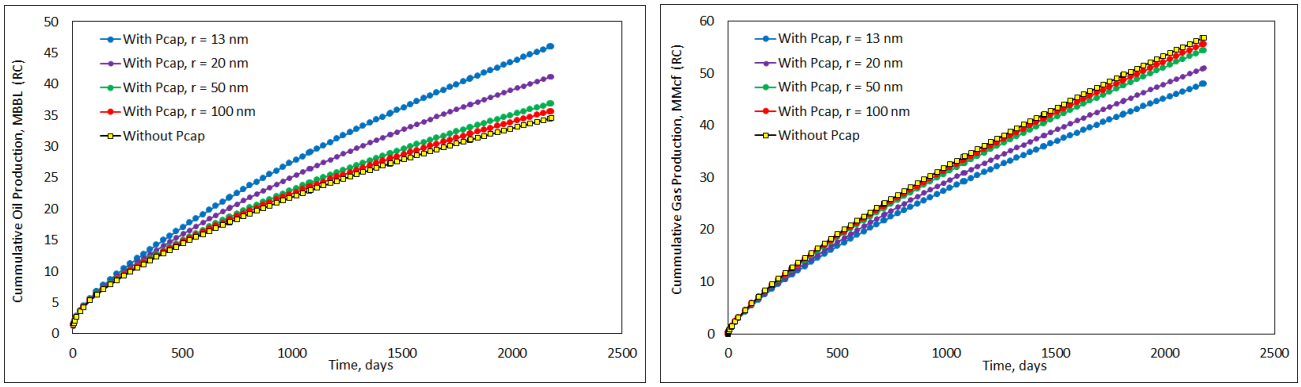

Figure 6 - 6 Cumulative production with reservoir pressure set below P_b of Bakken fluid system at various pore radii

6.3 Impact of Pore Size Distribution on Hydrocarbon Production and Recovery

According to Sondergeld (2013), shale reservoirs exhibit hydrocarbon storage and flow characteristics that are *"uniquely tied to nano-scale pore throat and pore size distribution"*. A typical shale reservoir can contain pores of size ranging from 2-5 nm (nano-pores) to >100 nm (macro-pores) (Alharthy, 2013)**.** Even though we ran cases in the previous section using same pore size throughout the reservoir to investigate the fundamentals of capillary pressure's dependence on pore radius, in reality, the influence of capillary pressure is expected to be associated to the specific pore size distribution (PSD) in the reservoir. Two PSD cases were thus investigated.

6.3.1 Pore Size Distribution 1

(Kuila, 2012) compiled pore size distribution of various shale samples, as shown in Figure 6-7. Based on the interpretation offered by Mavor (2013) on the work of Kuila (2012), in a typical shale reservoir:

- Roughly 80-87% of the pore space is occupied by pores bearing an average radius greater than 100 nm.
- 10-15% of pore space have an average radius of about 25 nm.
- 3-5% of pore space have average pore radius of 2-3nm

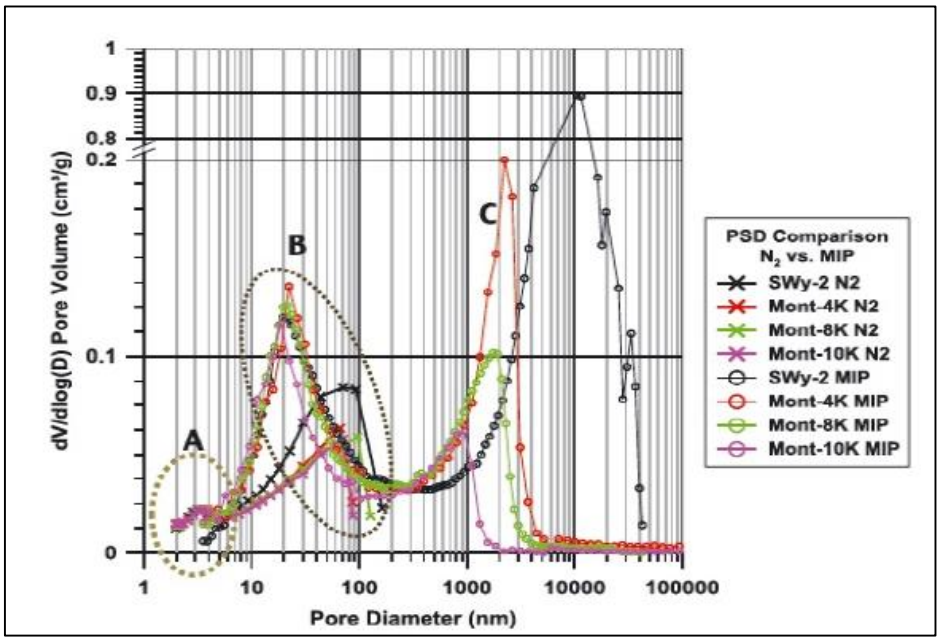

Figure 6 - 7 Pore size distribution of various shale sample (Kuila, 2012). Taken from Alharthy (2013)

A synthetic pore size distribution was created using the pattern explored by Kuila (2012), but with pore radii multiplied by a factor of 2 to give pessimistic results.1500 hundred grid blocks of the reservoir where distributed as shown Figure 5-8, that is, 5% of the blocks were set to pore sizes in the range of 1-10 nm, 15% in 10-100 nm and the rest of 80% in the category of pore sizes to be greater >100 nm. Figures 6-8 and 6-9 show the distribution of pore sizes in these three different ranges. Similar to the work of Kuila (2012), the medians of the three distribution are ~4 nm, ~30nm and ~2250 nm. Once 1500 pore sizes were generated, each grid block was randomly assigned a pore size value from this generated list.

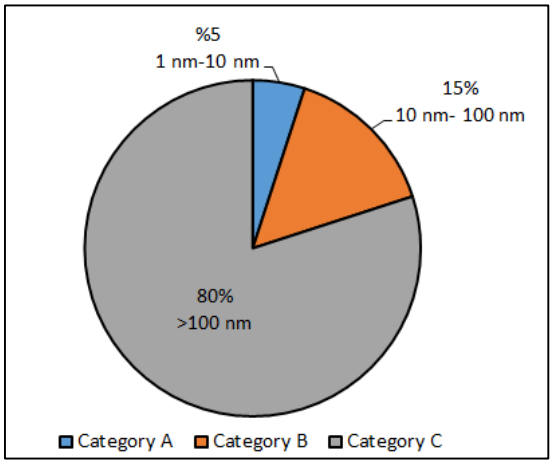

Figure 6 - 8 Distribution of pores size used in simulation (adopted from Kuila (2012) with pore radius multiplied by 2)

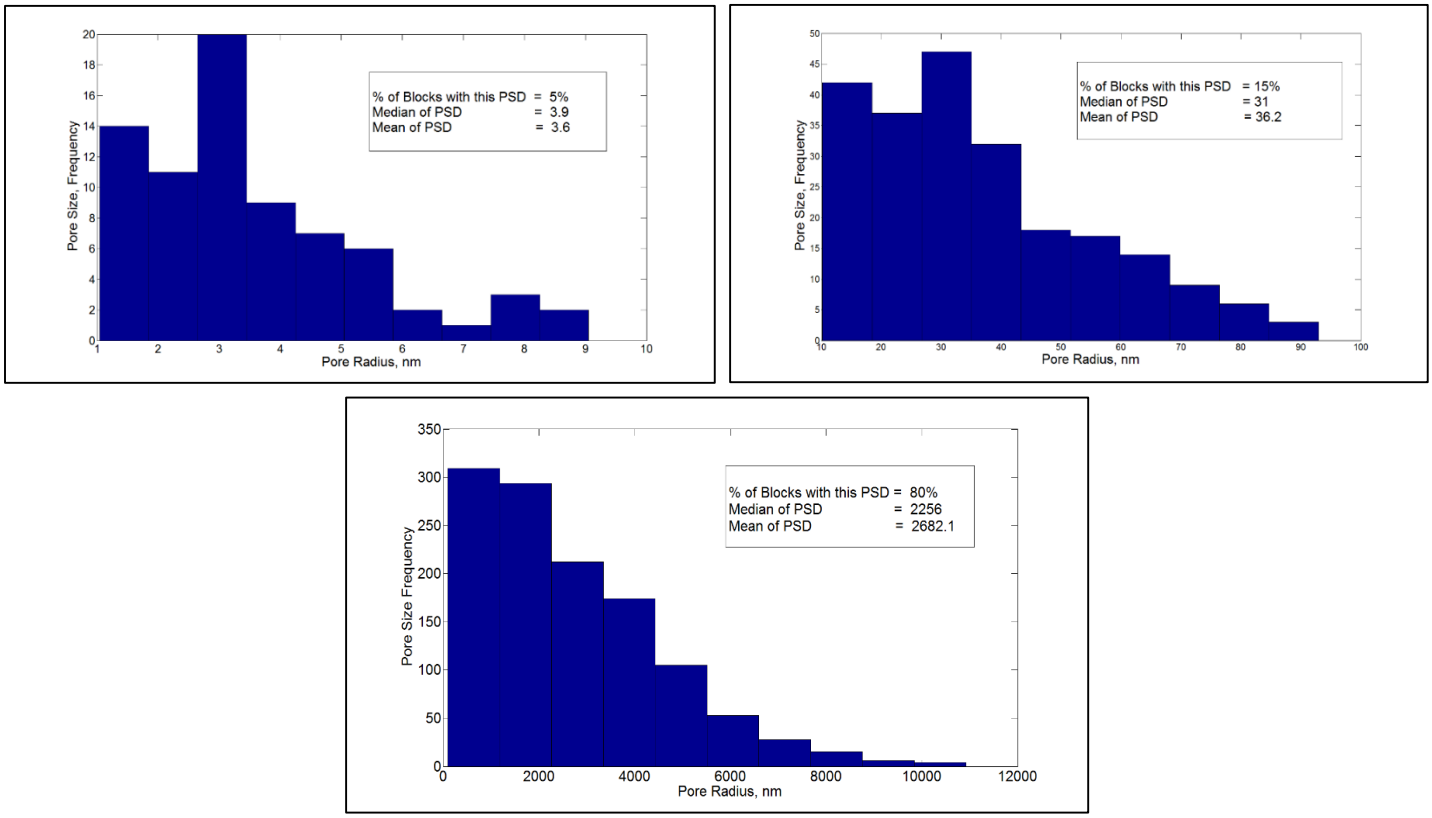

Figure 6 - 9 Distribution of pore sizes in various ranges

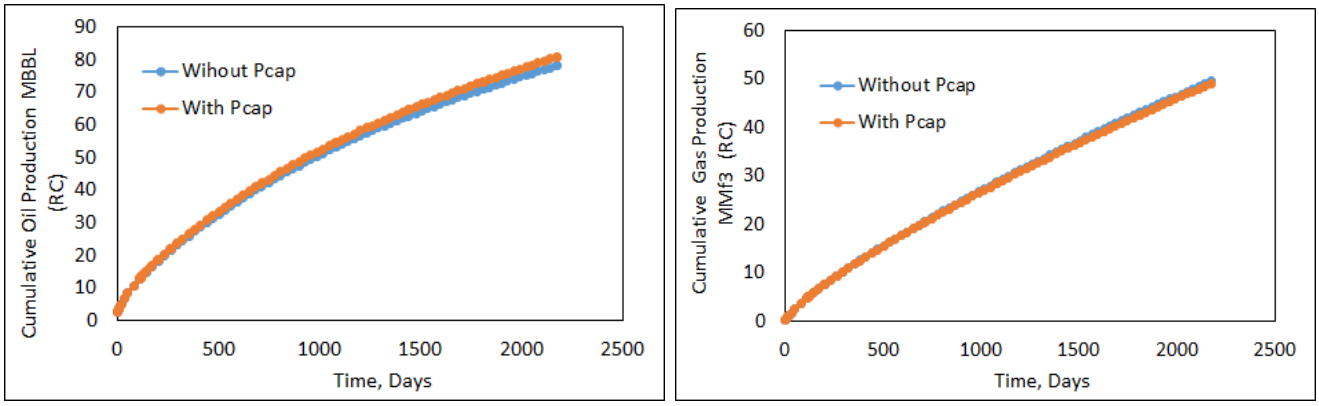

Figure 6- 10 Cumulative oil and gas production at PSD 1

The initial reservoir pressure was set to 2500 psia (below the bubble point pressure) and FBHP set to 100 psia. Figure 6-10 shows cumulative oil and gas production with and without capillary pressure, respectively. The increase in cumulative oil production after running the simulation for ~6 years is only 3.331%, while the decrease in gas production is 0.98%. This is because a great proportion of pores fall in the macro-pore domain where the effect of confinement is negligible.

6.3.2 Pore Size Distribution 2

It has been cited by several authors that average pore radius of Bakken field is less than 100 nm (Firincioglu, 2014) (Wang, 2013) (Nojabaei, 2012). Therefore, in reality the porportion of nano and meso-pores is expected to be much larger than that indicated in Kuila's derived PSD. Figure 6-11 shows yet another PSD synthetically created. Pore sizes ranging from 10 nm to 100 nm form 60% in this PSD.

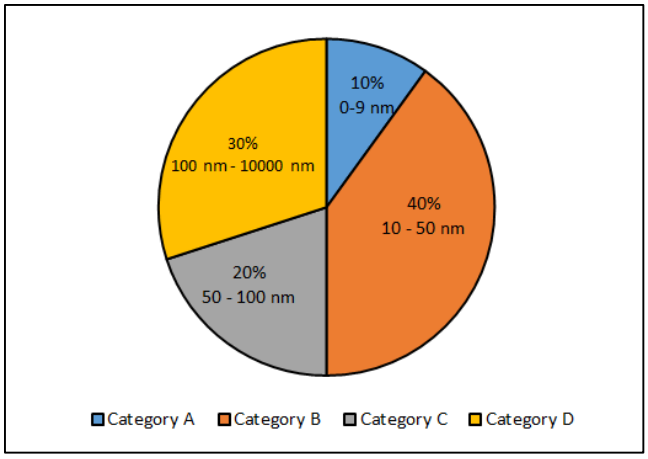

Figure 6 - 11 Pore size distribution with a larger proportion of meso-pores

Simulation was run for ~5.5 years using the generated PSD at a reservoir pressure of 2500 psia and a FBHP of 100 psi. Figures 6-12 and 6-13 show the differences in the daily and cumulative production. Cumulative oil production showed an increase of 10%, while cumulative gas production showed a decrease of 4%. It is interesting to compare this more realistic case with the one studied in section 6.2.2 where the reservoir was considered to be homogenously distributed with only 13 nm sized pore radii and the initial reservoir pressure was 2000 psia. The difference in cummulative oil production after ~6 years was found to be a staggering 33.2% and while in cumulative gas production to be 15.6%. Thus in reality, the impact of capillary pressure is uniquely tied to the PSD of the resevoir.

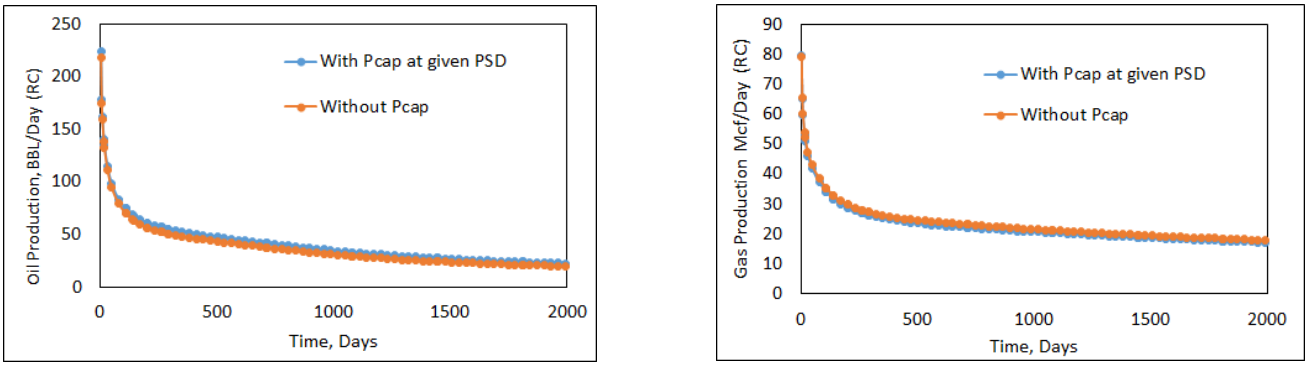

Figure 6 - 12 Daily production rates at PSD 2

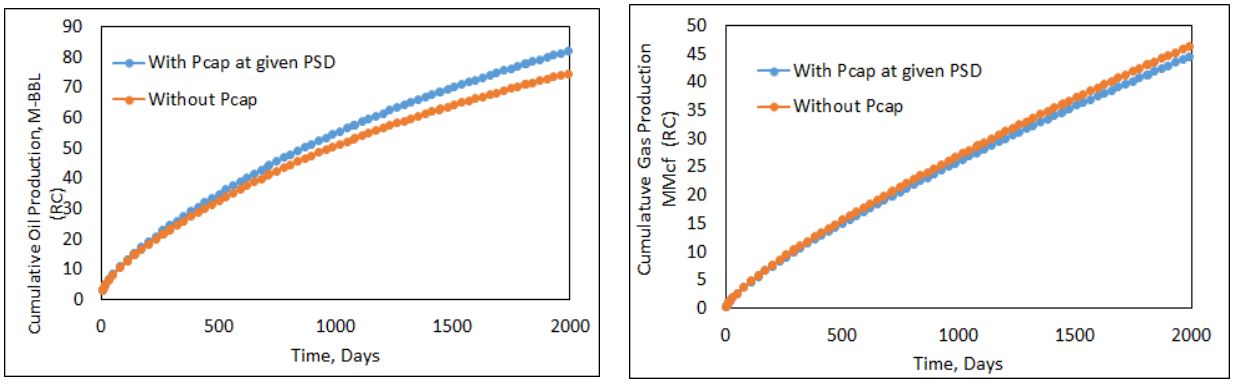

Figure 6 - 13 Cumulative production at PSD 2

6.4 Impact of Fluid Composition on Capillary Pressure

Unlike single phase shale gas reservoirs, liquid rich fluids in shale have an obvious added complexity resulting from multiple phases. Many shale reservoirs such as the Eagle Ford, contain a wide spectrum of hydrocarbon fluids. According to Haghshenas (2014) the fluid type in shale reservoirs can range from "low GOR black oil to volatile, rich and lean gas condensates, wet gas and even dry gas". Additionally, these fluid compositions have also been shown to vary spatially within the play (Haghshenas, 2014). Therefore fluids must be characterized accurately in order to predict fluid production from liquid rich shale reservoirs.

In this section, we investigate the impact of varying fluid composition on capillary pressure. It is very likely that capillary pressure's influence on production using one fluid composition system will differ from the other. We did a similar investigation using simple binary mixtures in Chapter 4. In this chapter, we studied this same effect by varying the composition of Bakken fluid. This was done by increasing the percentage of each of the 8 elements in Bakken fluid by 50% turn by turn, while normalizing the others, so as to check which set of components caused the greatest increase in the influence of capillary pressure. Table 6-2 lists the original and altered compositions of Bakken fluid.

Table 6 - 2 Original and altered compositions of Bakken fluid

Composition	C1	C2	C3	C4	C5-C6	C7-C12	C13-C21	C22-C80
Original	**0.36736**	**0.14885**	**0.09334**	**0.05751**	**0.06406**	**0.15854**	**0.0733**	**0.03704**
+50% C1	0.55104	0.12261	0.0671	0.03127	0.03782	0.1323	0.04706	0.0108
+50% C2	0.356728	0.223275	0.082708	0.046878	0.053428	0.147908	0.062668	0.026408
+50% C3	0.360693	0.142183	0.14001	0.050843	0.057393	0.151873	0.066633	0.030373
+50% C4	0.363252	0.144742	0.089232	0.086265	0.059952	0.154432	0.069192	0.032932
+50% CA	0.362784	0.144274	0.088764	0.052934	0.09609	0.153964	0.068724	0.032464
+50% CB	0.356036	0.137526	0.082016	0.046186	0.052736	0.23781	0.061976	0.025716
+50% CC	0.362124	0.143614	0.088104	0.052274	0.058824	0.153304	0.10995	0.031804
+50% CD	0.364714	0.146204	0.090694	0.054864	0.061414	0.155894	0.070654	0.05556

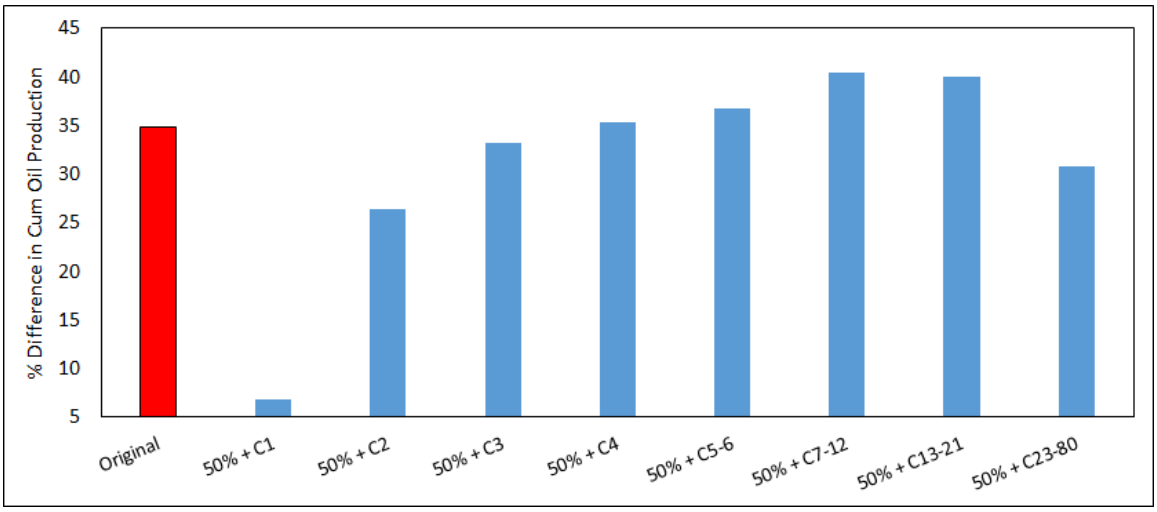

Figure 6 - 14 Impact of composition on capillary's pressure's influence on cumulative oil production

The simulation was run at a reservoir pressure below the bubble point pressure. Based on our findings, the magnitude of capillary pressure differs for different sets of compositions. Figure 6-14 shows the percentage difference in the cumulative oil production with and without capillary pressure at a fixed pore radius of 10 nm. The trend shows that capillary pressure's impact becomes greater as the percentage of mid-heavy components is increased, and starts dropping as the percentage of the heavy components increases. This effect could be best explained in terms of pressure temperature phase diagrams.

Nojabaei (2012) investigated the influence of capillary pressure on simple binary mixtures, as shown in Figure 6-14. They found that the influence of capillary pressure becomes more apparent "as the fluids become more immiscible. That is, C_3 is substituted with C_4 and C_4 with C_6, as long as the pressures remain relatively low". The effect of capillary pressure on the bubble point is decreased for $C_1 - C_{10}$ mixture because the bubble point pressures for that system become much higher, which reduces the density differences between liquid and vapor. The larger pressures therefore reduce the interfacial tension along the bubble point curve.

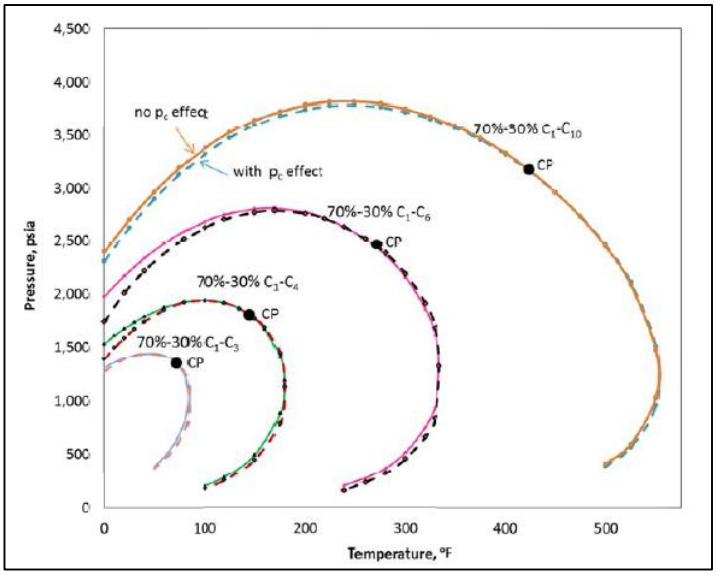

Figure 6 - 15 Phase envelopes for binary mixtures with and without capillary pressure (Nojabaei, 2012)

Extending these findings to Bakken fluid system, three composition sets were chosen, namely +50% C1 (lighter), +50% C7-C12 (mid-heavy) and +50% C23-C30 (heavy). Figure 6-16 shows the bubble point pressure curves of these three composition sets. Agreeing to the results shown in Figure 6-15, and findings of Nojabaei (2012), the +50% C7-C12 (mid-heavy) experiences the highest suppression in bubble point pressures based on its critical point position. Therefore, phase envelope's original shape (critical point position) plays a key role in determining the impact of capillary pressure.

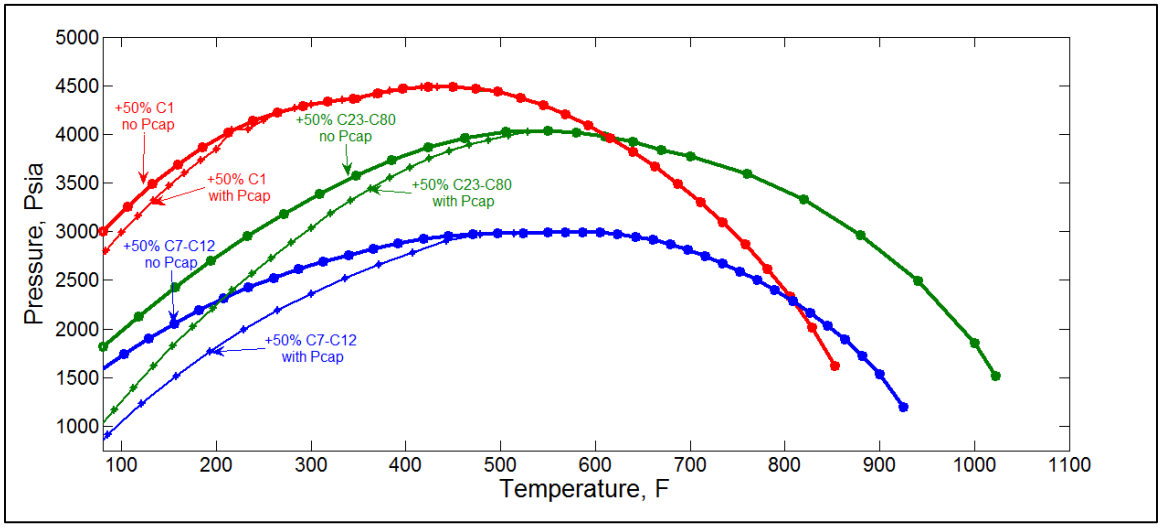

Figure 6 - 16 Phase envelopes of 3 altered Bakken fluid compositions: +50% C1 (lighter), +50% C7-C12 (mid-heavy) and +50% C23-C30 (heavy)

6.5 Impact of Critical Properties Shifts due to Confinement on Hydrocarbon Production

From the influence of capillary pressure, we now shift the discussion to the alteration of critical properties due to confinement in tight pore systems. Confined space or pore proximity effect alters the fluid properties and phase behavior (Singh, 2009) (Sapmanee, 2011) (Teklu, 2014). This has been discussed in detail in Chapter 2. This section follows the work of Teklu (2014) and then extends the study towards investigating the impact of critical properties shifts in realistic reservoir scenarios using AD-GPRS.

6.5.1 Impact of Critical Properties Shift due to Confinement on Fluid Phase Envelope

Singh (2009) used Grand Monte-Carlo simulation to study the impact of confinement on critical properties. He developed the following correlations for the shifts in critical tempertare and pressure-

$$\Delta T_c^* = \frac{T_{cb} - T_{cp}}{T_{cb}} = 0.9409\frac{\sigma_{LJ}}{r_p} - 0.2415\left(\frac{\sigma_{LJ}}{r_p}\right)^2 \quad \textbf{(6- 1)}$$

$$\Delta P_c^* = \frac{P_{cb} - P_{cp}}{P_{cb}} = 0.9409\frac{\sigma_{LJ}}{r_p} - 0.2415\left(\frac{\sigma_{LJ}}{r_p}\right)^2 \quad \textbf{(6- 2)}$$

Here $\sigma_{LJ} = 0.2443\sqrt[3]{\frac{T_{cb}}{P_{cb}}}$, which is Lennard Jones size parameter (collision diameter in nm), r_p is pore radius (nm), ΔT_c^* is relative critical temperature shift (dimensionless), T_{cb} is bulk critical temperature (K), T_{cp} is pore critical temperature (K), ΔP_c^* relative critical pressure shift (dimensionless), P_{cb} is pore critical pressure (atm) and P_{cp} is pore critical pressure (atm).

Table 6-3 lists the confinement parameters, critical property shifts and the subsequent confined critical properties of Bakken fluid components at a pore radius of 10 nm. Both critical temperature and pressure decrease under the influence of confinement.

Table 6 - 3 Confinement parameters and critical property shifts of Bakken fluid components at a pore radius of 10 nm

	C1	C2	C3	C4	CA	CB	CC	CD
σ_{LJ} (nm)	0.393043	0.448712	0.504328	0.548234	0.608306	0.700548	0.858597	1.047887
T_{cb}(K)	186.2978	305.5384	369.9834	421.7823	486.3773	585.1389	740.0528	1024.717
P_{cb}(atm)	44.57146	49.1285	41.89997	37.18439	31.3889	24.72382	16.98495	12.9369
ΔT_c^*	0.036608	0.041733	0.046838	0.050857	0.056342	0.064729	0.079005	0.095944
ΔP_c^*	0.036608	0.041733	0.046838	0.050857	0.056342	0.064729	0.079005	0.095944
T_{cp}(K)	179.4777	292.7873	352.6541	400.3315	458.9738	547.2633	681.5849	926.402
P_{cp}(atm)	42.93977	47.07822	39.93746	35.29329	29.62039	23.12346	15.64305	11.69568
σ_{LJ}/r_p	0.039304	0.044871	0.050433	0.054823	0.060831	0.070055	0.08586	0.104789

In order to study the impact of pore size on the critical property shifts of various components in Bakken fluid system, the σ_{LJ}/r_p ratio was computed for every pore radius (parameters for pore radius of 10 nm have been listed in Table 6-3). Figure 6-17 shows the plot of these critical shifts for Bakken fluid components at 4 different pore radii (points in same color share the same pore radius). As can be seen, the critical property shift increases as the molecules become heavier and the pore radius becomes smaller. Based on these findings, Teklu (2014) postulated that these shifts can be ignored for pore size > 30 nm.

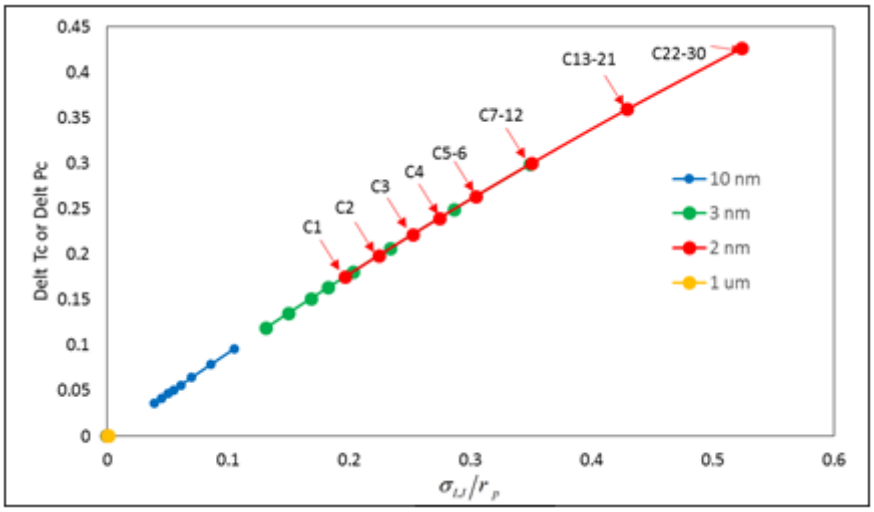

Figure 6 - 17 Impact of critical property shift as a function for Bakken fluid component

Using the new critical properties, Bakken fluid phase envelope was constructed using AD-GPRS. Figure 6-18 shows significant suppression of the entire phase envelope and a pore radius of 10 nm.

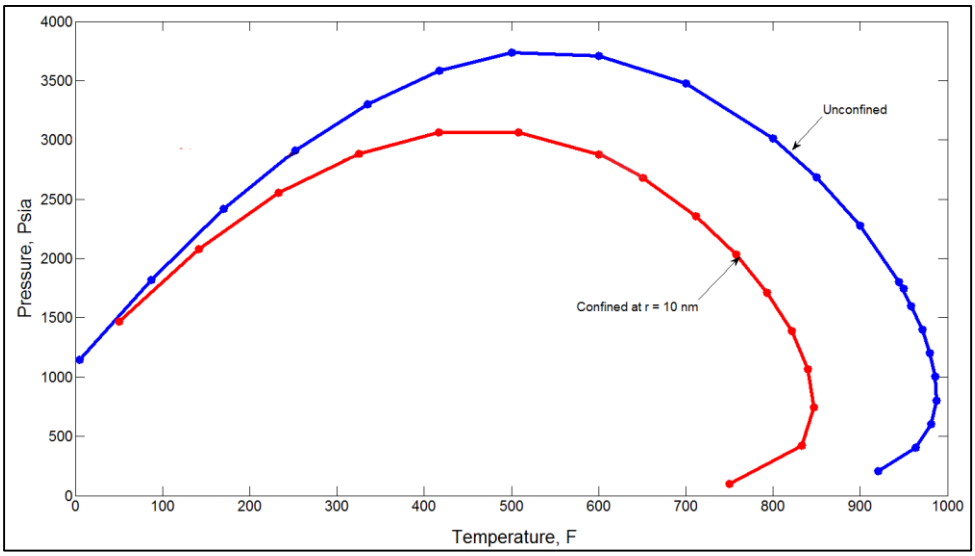

Figure 6 - 18 Suppression of Bakken fluid phase envelope due to shifted critical properties at pore radius of 10 nm

6.5.2 Impact of Critical Properties Shift due to Confinement on Hydrocarbon Production

After having studied certain key aspects of phase behavioral changes due to shifts in the critical properties, this investigation was extended to study the impact of confinement on hydrocarbon production in realistic reservoir set-up. The same model as described in Table 6-1 was used, but the fractures were removed because confinement effect is only felt in rock matrix. Figures 6-19 and 6-20 show that both oil and gas production increases. Similar trends were observed by Sanaei (2014) for Eagle Ford gas condensate system. They found that two-phase envelope shrinks due to decrease in pore size and "fluid starts to behave more like a dry gas". Sanaei, in the same work, also found that both condensate and gas viscosity decreased under confinement. This factor, as well as a significant decrease in condensate drop-out resulted in a "dramatic increase" in liquid production under confinement. They investigated different reservoir scenarios and obtained a maximum of 200% difference in condensate production prediction.

The cumulative production's trend shown in Figure 6-19 appears linear since a single well is producing from a very tight matrix with no fracture. A better approach would have been to relate the critical property shift to permeability and divide the reservoir in segments based on permeability. The impact of confinement should be absent in fractures.

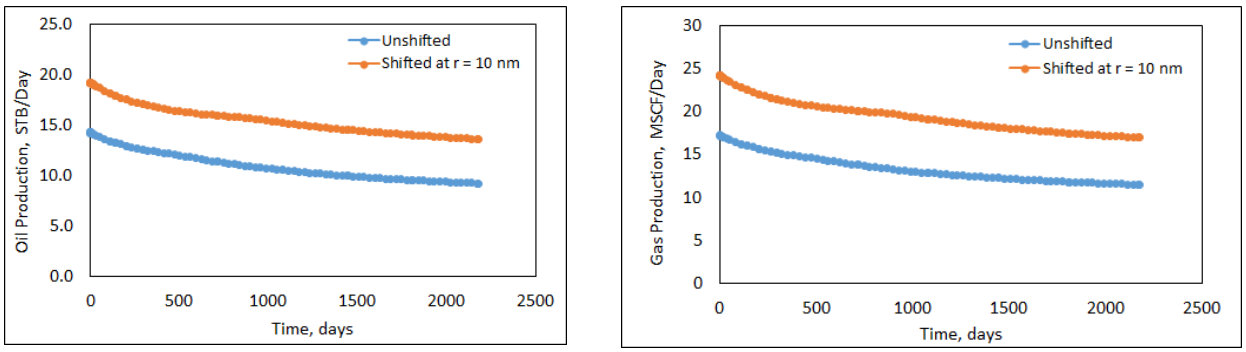

Figure 6- 19 Impact of critical properties' shift due to confinement on daily production rates

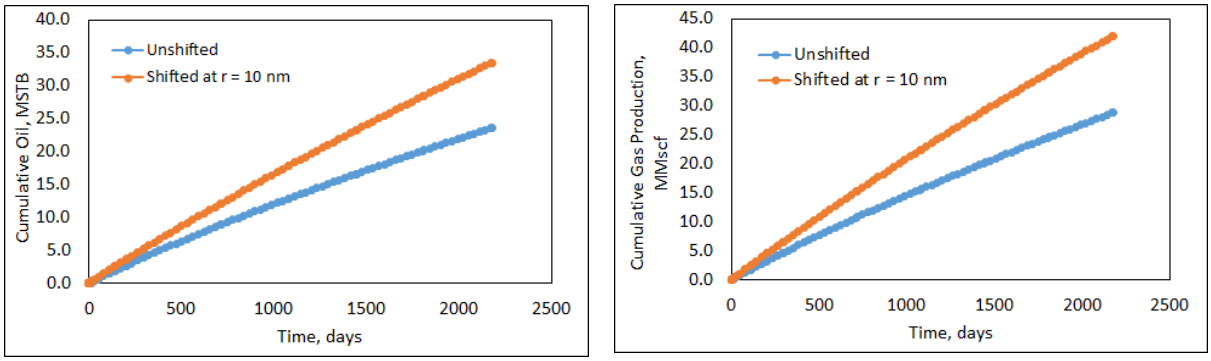

Figure 6- 20 Impact of critical properties' shift due to confinement on cumulative production

6.6 Summary

This chapter investigated the impact of confinement (capillary pressure and critical property shifts) on hydrocarbon production in realistic reservoir scenarios. In the presence of capillary pressure, the change in production was found to be zero when the reservoir pressure is above the fluid bubble point pressure. Capillary pressure was found to be a strong function of reservoir pressure, pore radius and fluid compositions. Correlations used for calculating critical property shifts showed that both critical temperature and pressure reduce as the pore size is decreased. It was shown that this reduction is greater for heavier components. Additionally, both oil and gas production showed an increase with the new shifted critical properties.

Chapter 7

Critical Fine details related to the Implementation of Capillarity for Tight Pores in Reservoir Simulators

This chapter involves discussion of some of the finer yet important details related to extending capillary pressure formulation in reservoir simulators. It is intended to highlight a few areas that need to be dealt with careful consideration so as to avoid potential inaccuracies. Some of these points can be extended to new frontiers of research in this area.

7.1 Impact of the Presence of Fractures on Influence of Capillary Pressure

As was mentioned in Chapter 6, the effect of confinement should only be felt in rock matrix and not in fractures. In this formulation, fractures can be considered as regions with infinite pore radius, to mitigate the effect of capillarity in them. Thus more the fractures, less is the influence of capillarity. Figures 7-1 and 7-2 show the error that might be caused if the 10 hydraulic fractures were not separately accounted for in flash calculations. The simulations have been run with initial reservoir pressure set below the bubble point pressure of Bakken fluid. Lines of same color indicate same pore radii. The error increases as the pore size decreases. Also, note that the reservoir set up used in this work is single porosity/permeability. In reality a typical shale reservoir is highly fractured and so natural fractures should be considered. A better approach would be a multiple porosity/permeability model with confinement related computations done only in the matrix region. It is thus important to properly characterize the fractures in a reservoir system so as to get a more accurate representation of production scenario under the influence of capillarity in tight pore systems. Same goes with the impact of confinement on critical properties' shifts. A good approach can be to set confinement effect to zero in high permeability regions.

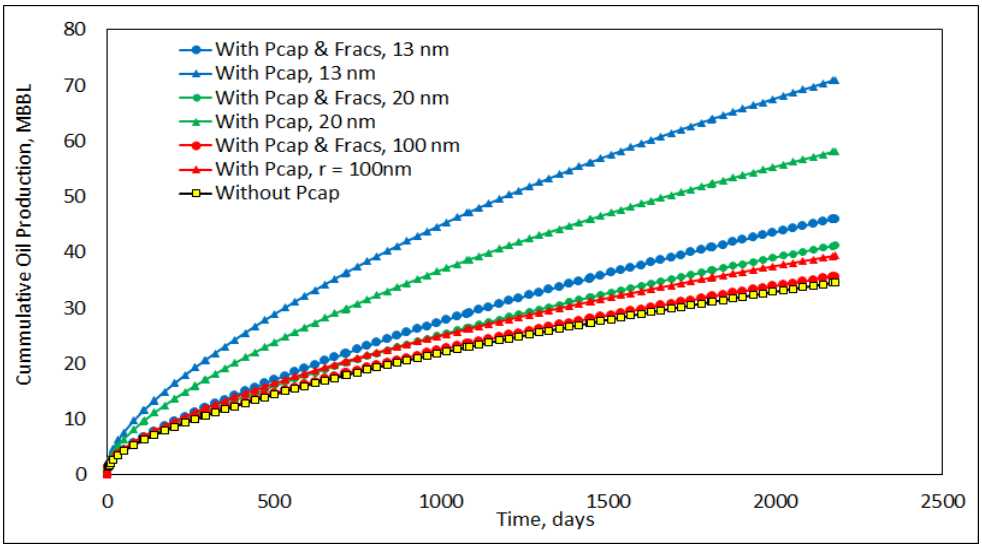

Figure 7- 1 Differences in cumulative oil production at different pore radii when the flash is incorrectly modified in both matrix and fractures, and when modified only in the matrix

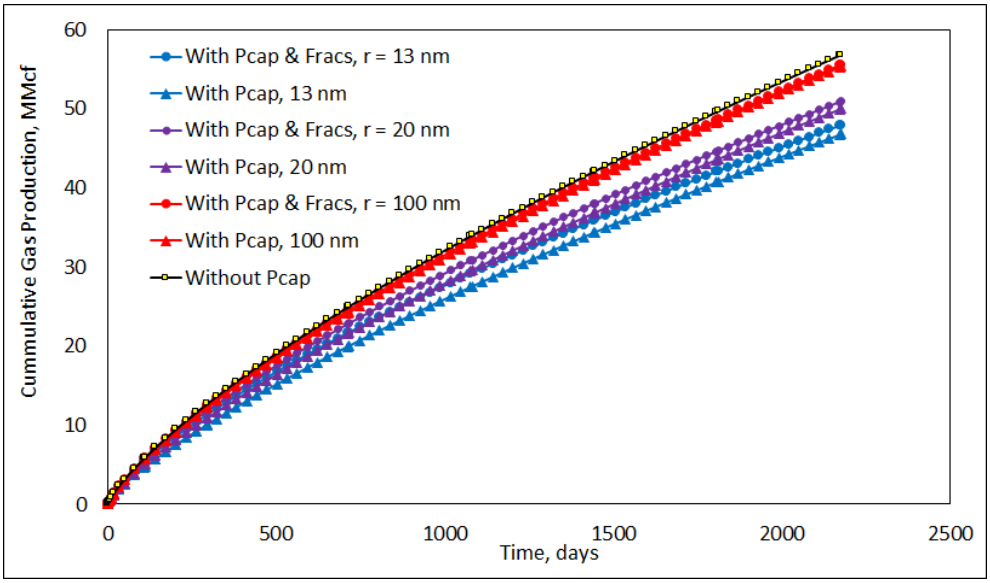

Figure 7- 2 Differences in cumulative gas production at different pore radii when the flash is incorrectly modified in both matrix and fractures, and when modified only in the matrix.

7.2 Introducing relationship between Permeability, Porosity and Pore Radius

Another simplification often done when dealing with extending the impact of confinement on tight pores is to fix the permeability, irrespective of the pore radius. In reality however, permeability, porosity and pore radius are all related. Reducing the pore size should decrease the permeability. Several attempts were made to study the influence of capillarity after linking these key parameters during the course of this work, and some key conclusions derived that are open to future research work. Table 7-1 shows pore radii calculated against permeability at a fixed porosity of 0.06 using correlations developed by Carman (1937), Kozeny (1927) and Nelson (1994). This table has been adopted from Wang (2013).

Table 7- 1 Pore size values against permeability Carman (1937), Kozeny (1927) and Nelson (1994). (Adopted from Wang (2013)

Pore Radius (nm)	Permeability (md)
50	0.0070
40	0.0046
30	0.0027
20	0.0012
10	0.0003

The above values were used to run simulation cases with the initial reservoir pressure set below the bubble point pressure. With every pore radius, its corresponding permeability, was used. Figures 7-3 and 7-4 show that both oil and gas show decrease in production with the reduction in pore size as the impact of reduction in permeability seems to be masking the impact of capillarity.

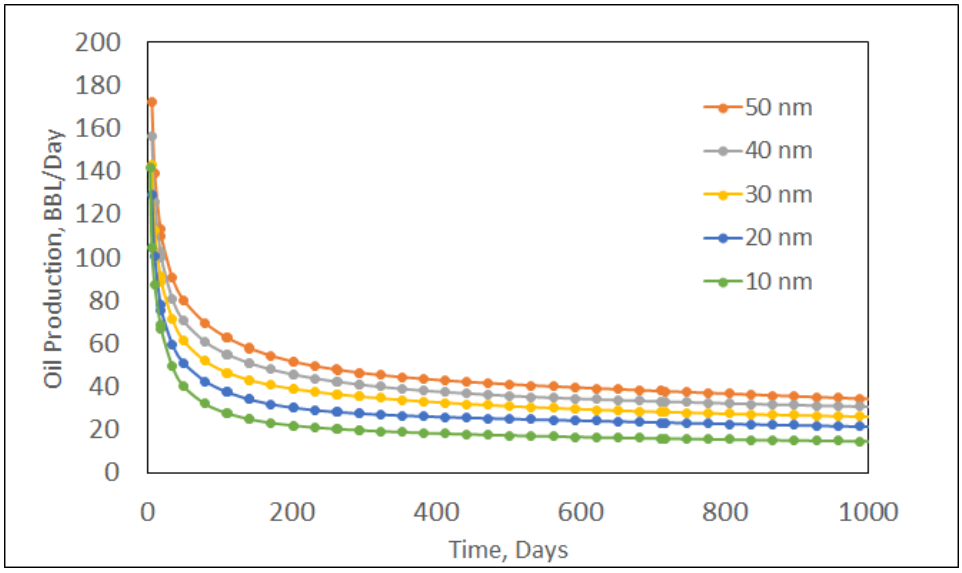

Figure 7- 3 Daily oil production rate at various pore radii using corresponding permeability values from Table 7-1

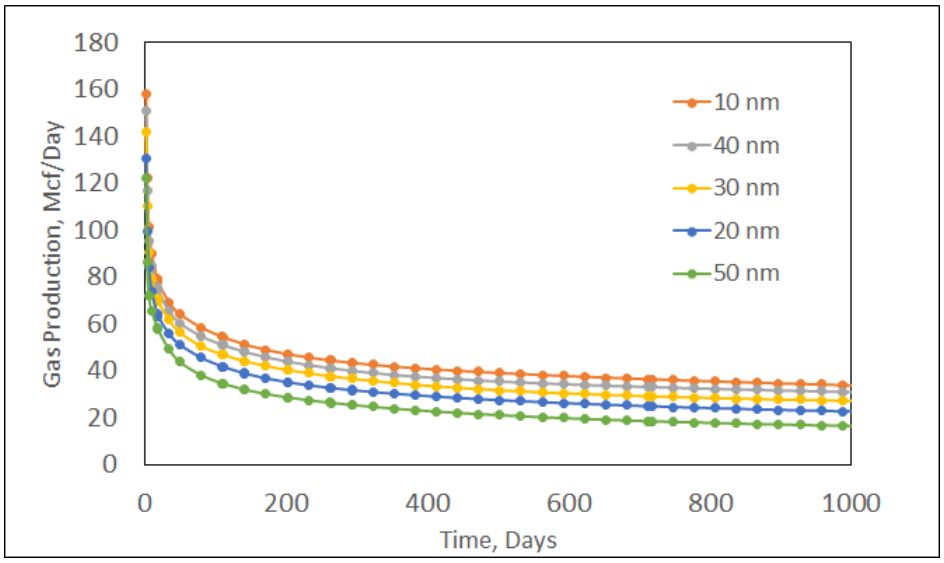

Figure 7- 4 Daily gas production rate at various pore radii using corresponding permeability values from Table 7-1

It is hard to comment what to expect in reality as it has been proven that permeability, porosity and pore radii correlations developed for conventional reservoirs do not apply to unconventional reservoirs (Hinai, 2013). In Table 7-1, the permeability corresponding to 50 nm is 0.007 md. According to Zhang (2011) the permeability of a typical tight reservoir ranges from 0.00001–0.0001 md. Thus 0.007 md easily falls outside the range of an ultra-tight reservoir such as shale. Additionally, in general measuring permeability in tight pores

is difficult. More research needs to be done in this domain so has to achieve a more realistic correlation.

A better approach would be to compute permeability, porosity and pore-size relationship for the specific shale formation under investigation. Sanaei (2014) used several samples from Eagle ford to obtain a linear relationship between pore size and permeability. This correlation was used in their computations related to the impact of critical property shifts due to confinement on hydrocarbon production.

Chapter 8

Conclusions and Future Work

8.1 Conclusions

This research aimed to explore some of the key physical fundamentals of confinement. The two phenomenon that may become significant in tight pore reservoirs are capillary pressure and critical property shift due to confinement, were investigated. Following are the main conclusions of this work:

1. Capillary pressure causes suppression in bubble point pressure and this suppression is a strong function of pore radius, fluid composition and reservoir pressure.
2. The suppression of bubble point leads to reduction in oil density and viscosity, and increase in gas density & viscosity.
3. The alteration of phase behavior due to the influence of capillary pressure leads to an increase in oil production, while it reduces gas production.
4. The influence of capillary pressure is absent when the reservoir pressure is above the bubble point pressure of the fluid. As the reservoir pressure falls below the bubble point, capillarity can have a significant impact on hydrocarbon production.
5. Reduction in pore radius causes an increase in capillary pressure. In one example, with a pore size of 13 nm (homogenously spread throughout the reservoir) and a reservoir and FBHP of 2000 psia and 100 psia, respectively, an increase of 33.2% in oil production at reservoir conditions, while a reduction of 15.6% in gas production was experienced.
6. It was also found that pore size distribution can have a huge impact on the overall magnitude of capillary pressure. Thus in one of the realistic pore size distribution cases, the increment in condensate and gas production due to capillarity, was obtained to 10% and 4% respectively, which is low when compared to 33.2% and 15.6% increment in cummulative oil and gas production obtained when the reservoir is assumed to comprise of pores of only 13 nm in size. Therefore the impact of capillary pressure is indeed uniquely tied to the pore size distribution of a given shale formation.
7. The other major factor that influences the magnitude of capillary pressure is fluid composition. It was found that the initial phase envelope shape and the critical point pressure and temperature play a significant role in determining the strength of capillarity.
8. Lastly it was shown that the shift in critical properties due to confinement increases as the pore size reduces and the fluid components become heavier. Critical property shifts cause an increase in both oil and gas production.

8.2 Future Work

1. As a part of reservoir management strategy, the reservoir pressure is often maintained above the bubble point, so that gas remains dissolved in oil, thus reducing its viscosity and increasing oil recovery. It was shown that capillarity, on the other hand, can have a significant positive impact on oil production as the pressure falls below the reservoir pressure. Since the well density in shale reservoirs is far greater than in conventional reservoirs, these two seemingly opposite phenomena, both of which lead to an increase in oil production, can form an interesting reservoir optimization/management study, so as to maximize oil recovery from the reservoir. The impact of this phenomena on field development decisions should be further investigated.

2. It was also shown that the presence of fracture can reduce the influence of capillary pressure on production. A single porosity/permeability model was used in this research and thus only hydraulic fractures were considered in the system. In reality, shale reservoirs are massively fractured. Therefore a more realistic approach towards describing the influence of capillary pressure would be a multi-porosity/permeability model, where capillary pressure is significant only in the matrix.

3. Water saturation was set to zero in this work. Though this may be a reasonable approach for Bakken reservoir (Nojabaei, 2012), for some reservoirs it may not be appropriate. Nojabaei (2014) presented some interested method to extend capillary pressure calculation in tight pores to 3 phase systems.

4. The impact of heterogeneity was not tested in this work. Since capillary pressure is a function of both phase densities and pore radius, heterogeneity can have considerable impact on capillary pressure. This should be investigated further.

5. Since adsorption, osmotic pressure effects and capillarity have all be shown to be of importance in tight pore in literature, it will be interesting to see the net effect of all these forces combined, on hydrocarbon production and recovery.

References

Alharthy, N. S., 2013. *Multiphase Compositional Modelling in Small Scale Pores of Unconventional Shale Reservoirs*. SPE Annual Technical Conference and Exhibition, New Orleans, SPE 166306.

Ambrose, R. J., 2010. *New Pore Scale considerations for shale gas in place calculations.* Pittsburg, Pennsylvania, SPE 131772, SPE Unconvnetional Gas Conference.
Anon., 2012. Spectrum of pore types and networks in mudrocks and a descriptive classification of matrix related mud rock pores.

Ashour, I., 2011. *Applications of Equations of State in the Oil and Gas Industry.* Oman: Department of Petroleum and Chemical Engineering College of Engineering, Sultan Qaboos University.

Ashraf, M., 2015. *The Global Quest for Light Tight Oil: Myth or Reality?,* s.l.: Schlumberger Petrotechnical Services.

Ayirala, S., 2006. A new Parachor model to predict dynamic interfacial tension and miscibility in multicomponent hydrocarbon systems. *Colloid and Interface Science,* Issue 299, pp. 321-331.

Blasingame, T., 2013. *Reservoir Engineering Aspects of Unconventional Reservoirs.* Texas, USA, Analysis of Reservoir Performance for Unconventional Gas Condensate Reservoirs, Schlumberger CONDENFEST Webinar.

Brock, H.L. *Surface tension and the principle of corresponding states,* AIChE J. 1 (1955) 174.

Bustin, 2008. *Impact of Shale Properties on Pore Structure and Storage Characteristics.* Fort Worth, Texas, SPE Shale Gas Production Conference.

Carey, B.S. *The gradient theory of fluid interfaces,* Ph.D. dissertation, University of Minnesota, Minneapolis, 1979.

Carman, 1937. Fluid flow through granular beds. *Transaction, Institution of Chemical Engineers, London,* Volume 15, p. 150–166.

Chandra, S., 2014. Properties of Materials Confined in Nano-Pores. *Department of Physics, Banaras Hindu University, Varanasi,* Volume 221 - 005, India.

Clever. H.L. J. Chem. Eng. Data 8 (1963) 291.

Colorado Oil and Gas Association. 2013. Oil Shale vs. Shale Oil. Denver, CO, USA. http://www.coga.org/pdf_Basics/Basics_OilShale.pdf

Devegowda, D., 2012. *Phase Behvaiour of Gas Condensates in Shale due to Pore Proximity Effects: Implications for transport , reserves and well productivity.* San Antonio, Texas, SPE 160099, SPE Annual Technical Conference and Exhibition.

Dhananpal, 2014. *Phase Behaviour and Storage in Organic Shale Nanopores: Modeling of Multi-component Hydrocarbons in Connected Pore Systems and Implications for Fluids in Place Estimates in Shale Oil and Gas Reservoirs*. s.l., SPE 169008, SPE Unconventional Resources Conference.

EIA, 2013. *Technically Recoverable Shale Oil and Shale Gas Resources: An Assessment of 137 Shale Formations in 41 Countries Outside the United States*, Washington DC: US Energy Information Adminstration - Independant Statistics and Analysis.

Fan, Li. 2005. Understanding Gas-Condensate Reservoirs, Schlumberger. Oil Field Review, Texas, USA

Fine, K., 2009. *Bakken Water Opportunites Assesment - Phase 1*, North Dakota: North Dakota Industrial Commission, Oil and Gas Research Council.

Firincioglu, T., 2014. *PhD Thesis, Bubble Point Suppression in Unconventional Liquid Rich Reservoirs and its Impact on Oil Production*, Colorado: Colorado School of Mine.
Geology, O. &. G., 2010. *Oil and Gas Window*, s.l.: http://oilandgasgeology.com/.

Firoozabadi A., 1999, Thermodynamics of Hydrocarbon reservoirs, McGraw-Hill, NY

Gmehling, J. 2012. *Chemical Thermodynamics for Process Simulation*. Germany

Grguri. 2003. *Excess molar volume of acetonitrile + alcohol systems at 298.15 K. Part II: Correlation by cubic equation of state.* J. Serb. Chem. Soc. 68(1)47–56. JSCS–3019

Gordon, D., 2012. *Understanding Unconventional Oil Resources*, s.l.: Energy and Environment, Carnegie Papers.

Haghshenas, B., 2014. *Simulation of Liquid-Rich Shale Gas Reservoirs with Heavy Hydrocarbon Fraction Desorption.* Woodlands, USA, SPE 168968, SPE Uncoventional Resources Conference.

Hamada, 2007. Phase equilibria and interfacial tension of fluids confined in narrow pores. *J. Chem Physics*, 127 (8)(084908-1-084908-9).

Hinai, A., 2013. Permeability Prediction from Mercury Injection Capillary Pressure: An Example from the Perth Basin, Western Australia. *APPEA Journal,* Issue 53:, pp. pp. 31-36..

Honarpour, 2013. *The Critical role of rock and fluids in Unconventional Shale reservoir Performance.* Stanford, Presentation delivered at Stanford University, Energy Resources Engineering department weekly meetings.

Ismail, M. A., 2010. *Field Observation of Gas Condensate Well Testing,* Stanford, California: MS Report, Energy Resources Engineering Department, Stanford University.

Ismail, M. A., 2014. *An Investigation of Gas-Condensate Flow in Liquid-Rich Shales,* SPE 169021. SPE Unconventional Resources Conference, 1-3 April, The Woodlands, Texas, USA

Jiang, J., 2006. Capillary phase transitions of linear and branched alkanes in carbon nanotubes from molecular simulation. *Langmuir,* Volume 22, p. 7391.

Kovscek, A., 1996. *Thermodynamics of Fluid Phase Equilibria, Class Notes.* Stanford, California: Stanford University.

Kozeny, 1927. Ueber kapillare leitung des wassers im boden. *Sitzungsber Akad, Wiss., Wien,,* Volume 136(2a), pp. 271-306.

Kuila, U., 2012. *Application of Knudsen Flow in Modelling Gas-Flow in Shale Reservoirs.* Hyderabad, 9th Biennial International Conference and Exposition on Petroleum Geophysics.

Kuila, U. 2013. *Specific surface area and pore-size distribution in clays and shales.* Geophysical Prospecting, 61(2):341-362

Kuz, Z. a., 2002. Van der Waals equation of state for a fluid in a nanopor. *Physical Review,* Issue E 65, pp. 021110(1-4).

Loucks, R., 2012. Spectrum of pore types and networks in mudrocks and a descriptive classification for matrix-related mudrock pores. *The American Association of Petroleum Geologists,* Volume http://aapgbull.geoscienceworld.org/content/96/6/1071.figures-only.

Kwak. 1986. *Van Der Waals Mixing Rules for Cubic Equation of State*. Department of Chemical Engineering, University of Illinois, Chicago.

Lewis. 1923. *Thermodynamics and the Free Energy of Chemical Substances.* New York: McGraw-Hill Book Co., Inc.

Macleod, D.B. *On a relation between surface tension and density***,** Trans. Faraday Soc. 19 (1923) 38.

Matar, A. 2009. *Chemical Engineering Thermodynamics II (0905323) 02 - The Molar Gibbs Free Energy & Fugacity of a Pure Component.* Chemical Engineering Department. University of Jordan.
http://libvolume2.xyz/biotechnology/semester4/biochemicalthermodynamics/fugacityandactivity/fugacityandactivitytutorial1.pdf

Mavor, M., 2013. *Reservoir Fluid Properties Required for Low-Permeability Oil Reservoir Analysis.* Vancouver, BC, Canada, Geoscience Technology Workshop, Hydrocarbon Charge Considerations in Liquid-Rich Unconventional Petroleum Systems, Search and Discovery Article #80363.

Ma, Y., 2013. *Modifying Van Der Waals Equation of State to Consider Influence of.* New Orleans, Louisiana, USA, SPE 166476, SPE Annual Technical Conference and Exhibition.

Ma, Y., 2014. *Using Simplified Local Density/ Peng Robinson Equation of State to Study the Effects of Confinement in Shale Formations on Phase Behavior.* Woodlands, Texas, USA, SPE 168986, SPE Unconventional Resources Conference.

McCarthy, 2011. K. *Basic Petroleum Geochemistry for Source Rock Evaluation*. Oilfield Review Summer, Schlumberger. Houston Texas

Michelsen, L., 1982. The Isothermal Flash Problem. Part I. Phase-Split alculation. *Fluid Phase Equilibria,* Volume 9, pp. 21-40.

Mitariten, G., 2005. *Molecular gate adsorption system for the removal of carbon dioxide and/or Nitrogen from coal bed abd coal mine methane.* Two Rivers Convention Centre, CO, Western States Coal Mine Methane Recovery and Use Workshop.

Nelson, 1994. Permeability-porosity relationships in sedimentary rocks. *The Log Analyst,* pp. pp 38 - 62.

Nelson, 2009, *Pore-throat sizes in sandstones, tight sandstones, and shales*: AAPG Bulletin, v.93, no.3 (March), pp.329-340, Figure 2. AAPG ©2009

Nojabaei, B., 2012. *Effect of Capillary Pressure on Fluid Density and Phase Behavior in Tight Pore Rocks and Shales.* San Antonio, Texas, SPE 159258, SPE Annual Technical Conference and Exhibition.

Nojabaei, B., 2014. *Effect of Saturation Dependant Capillary Pressure on Production in Tight Rocks and Shales: A compositionally-Extented Black Oil Formulation.* Charleston, WV, SUA, SPE 171028, SPE Eastern Regional Meeting.

Pedersen, K., 2007. *Phase Behaviour of Petroleum Fluids.* s.l.:CRC Press, Taylor and Francis Group.

Pederson, J. 2010. *The Oil and Gas Window*, Oil and Gas Geology

http://www.oilandgasgeology.com/oil_gas_window.jpg

Pitakbunkate, T., 2014. *Effect of Confinement on PVT Properties of Hydrocarbon in Shale Reservoirs.* Amsterdam. Netherlands, SPE-170685, SPE Annual Technical Conference and Exhibition.

Pouchot, F., 2013. *Shale gas, oil reshape world energy landscape,* s.l.: phys.org.

Rachford, H. H., 1952. Procedure for Use of Electronic Digital Computers in Calculating Flash Vaporization Hydrocarbon Equilibrium. *J Pet Technol,* SPE 952327(4 (10): 19, 3.).

Rajput, V., 2014. *Thermodynamically Consistent Modelling of Adsorption in Liquid Rich Shales.* Denver, Colorado, USA, SPE 169589 ,SPE Western North American and Rocky Montain Joint Regional Meeting.

Rotelli, F., 2012. *PhD Dissertation, Shale Reservoirs: Pore-Scale Flow Behaviour and its Effect on Production,* Milano, Italy: Politecnico Di Milano.

Sanaei, A., 2014. *Production Modeling in the Eagle Ford Gas Condensate Window: Integrating New Relationships between Core Permeability Pore Size and Confined PVT* Properties, SPE 169493, SPE Western North American and Rocky Mountain Joint Regional Meeting. Denver, Colorado, USA

Sanaei, A., 2014. *Effect of Pore Size Distribution and Connectivity on Phase Behavior and Gas Condensate Production From Unconventional Resources.* Woodland, Texas, SPE 168970, SPE Unconventional Resources Conference.

Sapmanee, K., 2011. *Effects of Pore Proximity on Behavior and Production prediction of Gas/Condensate,* Oklahoma: MS thesis, Mewbourne School of Petroleum and Geological Engineering, University of Oklahoma.

Schaaf, S. A., 1961. High Speed Aerodynamics and Jet Propulsion. *Princeton University Press,* Volume vol 8, section H .

Sclumberger. 2015, T*he Global Quest for Light Tight Oil: Myth or Reality?* https://www.sbc.slb.com/Our_Ideas/Energy_Perspectives/1st%20Semester13_Content/1st%20Semester%202013_Global.aspx

Shirangi, 2015. Closed-loop field development under uncertainty by use of optimization with sample validation. *SPE Journal,* Issue SPE 163631 PA.
Singh, S., 2009. Vapor-Liquid Phase Coexistence, Critical Properties and Surface Tension of Confined Alkanes. *J. Phys. Chem. C,* pp. 113, 7170-7180.

Slatt, R., 2011. Pore types in the Barnett and Woodford gas shales: Contribution to understanding gas storage and. *AAPG Bulletin,* Volume 95, pp. 2017-2030.

Sondergeld, C., 2013. *Petrophysical considerations in evaluating and producing shale gas resources.* Pittsburgh, Pennsylvania, SPE 131768, SPE Unconventional Gas Conference.

Sudgen, *The variation of surface tension with temperature and some related functions* J. Chem. Soc. 25 (1924) 32.

Teklu, T., 2014. *Phase Behaviour and Minimum Miscibility Pressure in Nanopores.* Denver, SPE 168865, Unconventional Resources Technology Conference .

Teklu, T., 2014, Phase behavior and minimum miscibility pressure in nanpores, SPE Reservoir Evaluation and Engineering. SPE 168865

Thijssen, J. 2013. *e-study guide for: Computational Physics.* 2nd Edition.

Travalloni, 2010. Critical behavior of pure confined fluids from an extension of the van der Waals equation of state. *Chemical Engineering Science*, pp. 3088-3099.

Travalloni, s., 2014. Phase equilibrium of fluids confined in porous media froman extended Peng–Robinson equation of state. *Fluid Phase Equilibria,* Issue 362, pp. 335-341.

UGM, S. U. G. M., 2014. *Oil Shale,* s.l.: http://spe-sc.ft.ugm.ac.id/w/source-rock-and-kerogen/.

van der Waals 1873. *On the Continuity of the Gaseous and Liquid States* (doctoral dissertation). Universiteit Leiden.

Vidal, J. 1997. *Thermodynamics- Applications in Chemical Engineering and Petroleum Industry*.

Wang, Y., 2013. *Compositional Modelling of Tight Oil using Dynamic Nanopore Properties.* New Orleans, Loisiana, USA, SPE 166267, SPE Annual Technical Conference and Exhibition.

Wilson, G., 1969. *A Modified Redlich-Kwong Equation-of-State, Application to General Physical Data Calculations.*. Cleveland, Ohio, AIChE Natl.
Zhang, X., 2011. Sensitivity analysis of hydraulically fractured shale gas reservoirs. *Uncertainty analysis and reservoir modeling,* Volume AAPG Memoir 96, p. p. 281–287.

Zhang, Y., 2013. *Critical Evaluation of Equations of State for Multicomponent Hydrocarbon Fluids in Organic Rich Shale Reservoirs.* Denver, Colorado, SPE 168812.

Appendix A

A. Modified Flash Algorithm to Incorporate Capillary Pressure[3]

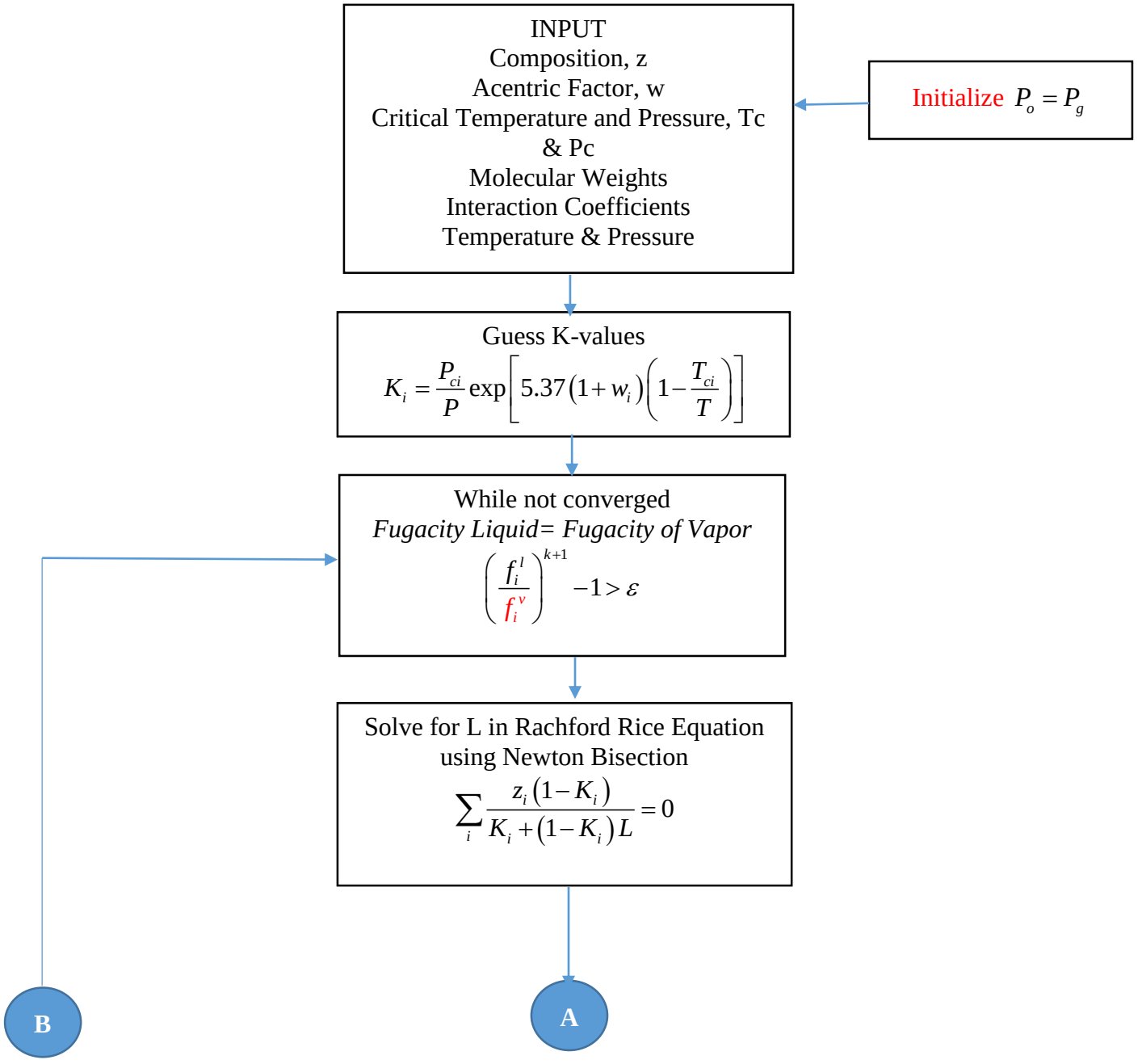

[3] The symbols highlighted in red color are the ones which will have to be modified to incorporate different phase pressures.

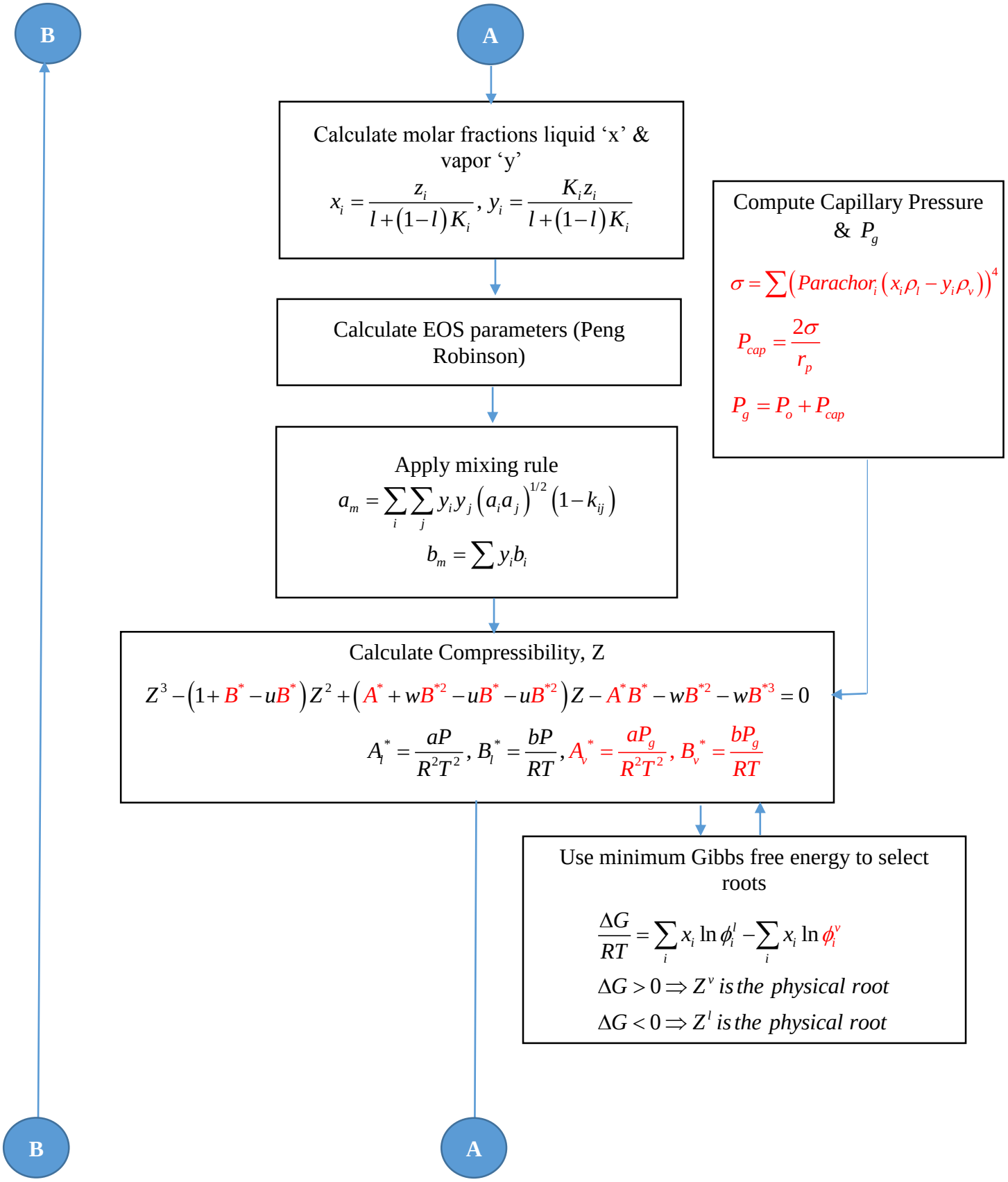
B
A
Calculate molar fractions liquid 'x' & vapor 'y'
$x_i = \frac{z_i}{l+(1-l)K_i}, y_i = \frac{K_i z_i}{l+(1-l)K_i}$
Calculate EOS parameters (Peng Robinson)
Apply mixing rule
$a_m = \sum_i \sum_j y_i y_j (a_i a_j)^{1/2}(1-k_{ij})$
$b_m = \sum y_i b_i$
Calculate Compressibility, Z
$Z^3 - (1 + B^* - uB^*)Z^2 + (A^* + wB^{*2} - uB^* - uB^{*2})Z - A^*B^* - wB^{*2} - wB^{*3} = 0$
$A_l^* = \frac{aP}{R^2T^2}, B_l^* = \frac{bP}{RT}, A_v^* = \frac{aP_g}{R^2T^2}, B_v^* = \frac{bP_g}{RT}$
Compute Capillary Pressure & P_g
$\sigma = \sum (Parachor_i (x_i\rho_l - y_i\rho_v))^4$
$P_{cap} = \frac{2\sigma}{r_p}$
$P_g = P_o + P_{cap}$
Use minimum Gibbs free energy to select roots
$\frac{\Delta G}{RT} = \sum_i x_i \ln \phi_i^l - \sum_i x_i \ln \phi_i^v$
$\Delta G > 0 \Rightarrow Z^v$ is the physical root
$\Delta G < 0 \Rightarrow Z^l$ is the physical root
B
A

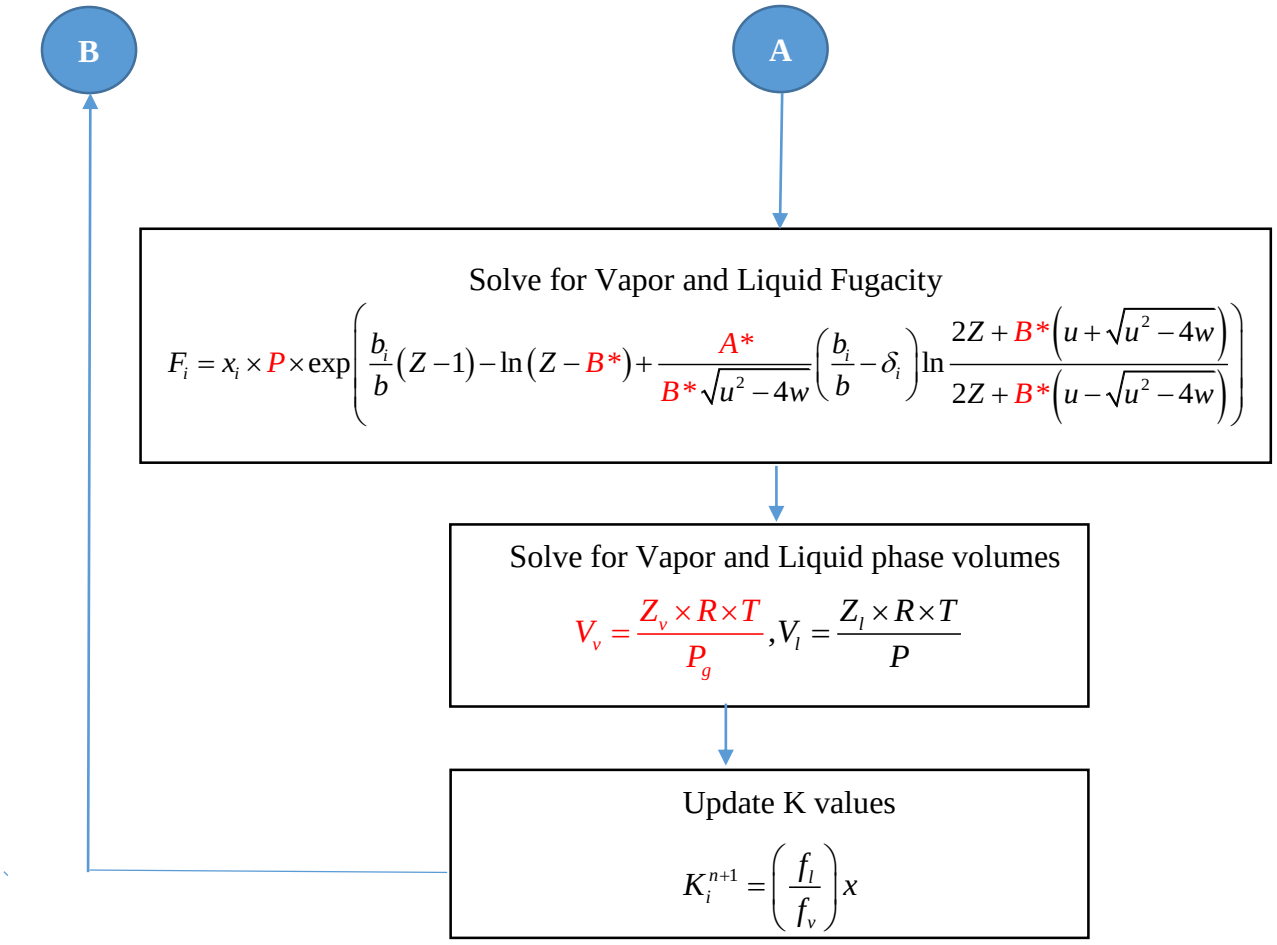
B
A
Solve for Vapor and Liquid Fugacity
$F_i = x_i \times P \times \exp\left(\frac{b_i}{b}(Z-1) - \ln(Z-B^*) + \frac{A^*}{B^*\sqrt{u^2-4w}}\left(\frac{b_i}{b} - \delta_i\right)\ln\frac{2Z+B^*\left(u+\sqrt{u^2-4w}\right)}{2Z+B^*\left(u-\sqrt{u^2-4w}\right)}\right)$
Solve for Vapor and Liquid phase volumes
$V_v = \frac{Z_v \times R \times T}{P_g}, V_l = \frac{Z_l \times R \times T}{P}$
Update K values
$K_i^{n+1} = \left(\frac{f_l}{f_v}\right)x$